

## Supporting Information for

# Characterization and Reactivity Study of Non-Heme High-Valent Iron–Hydroxo Complexes

Kritika Keshari,<sup>[a]</sup> Moumita Bera,<sup>[a]</sup> Lucía Velasco,<sup>[b]</sup> Sandip Munshi,<sup>[c]</sup> Geetika Gupta,<sup>[a]</sup>  
Dooshaye Moonshiram\*<sup>[b]</sup>, and Sayantan Paria\*<sup>[a]</sup>

<sup>a</sup>Department of Chemistry, Indian Institute of Technology Delhi, Hauz Khas, New Delhi-110016

<sup>b</sup>Instituto Madrileño de Estudios Avanzados en Nanociencia (IMDEA Nanociencia), Calle Faraday, 9,  
28049 Madrid, Spain.

<sup>c</sup>School of Chemical Sciences, Indian Association for the Cultivation of Science, 2A & 2B Raja S. C.  
Mullick Road, Jadavpur, Kolkata 700032

## Experimental Section

All of the chemicals used in this study were purchased from commercial sources like Sigma-Aldrich, TCI India, Alfa Aesar, Avra Synthesis, Spectrochem, and used as received. *Tris*(4-bromophenyl)ammoniumyl hexachloroantimonate (TBAH) was purchased from Sigma-Aldrich. Iron(III) perchlorate hydrate, tetramethylammonium hydroxide as 25% solution in methanol were purchased from Alfa Aesar and used as received. Anhydrous methanol and anhydrous acetonitrile were purchased from Sigma Aldrich, further deoxygenated by freeze-pump-thaw techniques and kept inside glovebox for use. Diethyl ether, hexane, benzene and tetrahydrofuran were purified over sodium/benzophenone, and deoxygenated by freeze-pump-thaw techniques. Isotope labelled water ( $\text{H}_2\text{O}^{18}$ ) was purchased from Cambridge Isotope Laboratories, Inc. Synthesis and manipulation of the iron complex were performed either in a nitrogen filled glovebox (Vigor Tech) or using standard Schlenk techniques. Gomberg's dimer was synthesized according to the literature procedure.<sup>1</sup> Oxidation potential of 4-X-2,6-di-*tert*-butylphenols ( $X = -\text{OCH}_3, -\text{CH}_3, -\text{CH}_2\text{CH}_3, -\text{C}(\text{CH}_3)_3, -\text{H}$ ) were taken from Karlin *et al.*<sup>2</sup> The  $\sigma_p^+$  values were taken from Hansch *et al.*<sup>3</sup>

**NMR Spectroscopy.** NMR spectra were recorded in a Bruker 500 MHz (DPX-500) or Bruker 400 MHz (DPX-400) NMR spectrometers. All chemical shifts are reported with respect to tetramethylsilane (TMS) as the internal standard.  $^1\text{H}$  NMR spectra of **1** & **2** were recorded as follows:

A 500  $\mu\text{L}$  of a 11.5 mM solution of complex **1** in  $\text{CD}_3\text{CN}$  was poured in an NMR tube inside the glove box and sealed with a septum. The  $^1\text{H}$  NMR spectrum of **1** was recorded in a 400 MHz instrument at 25  $^\circ\text{C}$ . Once the measurement is done, the NMR tube was taken out of the instrument and cooled in an acetone bath at  $-30$   $^\circ\text{C}$ . A 50  $\mu\text{L}$  solution of TBAH (115 mM) in  $\text{CD}_3\text{CN}$ , was slowly introduced in the NMR tube containing complex **1** and nitrogen gas was bubbled through a needle for a while to make the solution homogeneous and wait for 10 minutes to complete the reaction. The outside of the NMR tube was quickly wiped with a tissue paper and introduced in the precooled NMR probe and data was collected.

### Evans' Method.

A 500  $\mu\text{L}$  of a 13 mM solution of **1** in  $\text{CD}_3\text{CN}$  containing HMDS (internal standard) was introduced in a Wilmad screw-cap NMR tube. In a Wilmad coaxial insert stem, HMDS in  $\text{CD}_3\text{CN}$  was filled. The coaxial was then slowly introduced in the screw-cap NMR tube. The  $^1\text{H}$  NMR spectrum of the complex solution was taken at 298 K (Figure S5). Paramagnetic susceptibility of the iron complex was calculated using the following formula<sup>4</sup>:

$$\chi_p = \chi_0 + 3000\Delta\nu/4\pi\nu_0cM$$

Where,  $\chi_0$  = diamagnetic susceptibility,  $\Delta\nu$  = frequency shift of the  $\text{CH}_3$  protons of HMDS in Hz,  $\nu_0$  = frequency of the NMR instrument in Hz,  $c$  = concentration of the iron complex,  $M$  = molecular weight.

Diamagnetic susceptibility because of the iron complex, counter cations and solvents were deducted from the measured magnetic moment value to get paramagnetic susceptibility. Molar paramagnetic susceptibility was determined from the  $\chi_p$  value and molecular weight of iron complex. Effective magnetic moment ( $\mu_{\text{eff}}$ ) of **1** was calculated using the following equation<sup>5</sup>:

$$\mu_{\text{eff}} = (3k_{\text{B}}\chi_{\text{P}}T/N_{\text{A}}\beta^2)^{1/2} = (8 \times \chi_{\text{P}} \times T)^{1/2}$$

Where,  $k_{\text{B}}$  = Boltzmann's constant,  $T$  = Temperature,  $N_{\text{A}}$  = Avogadro's number,  $\beta$  = Bohr magneton. The ratio of  $3k_{\text{B}}/N_{\text{A}}\beta^2 \approx 8$ .

In a similar way, the magnetic moment of the intermediate (**2**) was determined. A 500  $\mu\text{L}$  of a 13 mM solution of **1** containing HMDS was prepared in  $\text{CD}_3\text{CN}$  and was introduced in a Wilmad screw-cap NMR tube under  $\text{N}_2$  atmosphere and the solution was cooled in a constant temperature bath at around  $-30\text{ }^\circ\text{C}$ . One equiv. of TBAH was introduced into the NMR tube and  $\text{N}_2$  gas was bubbled for a while to make the solution homogeneous at  $-30\text{ }^\circ\text{C}$ . After formation of **2**, a coaxial containing HMDS was quickly inserted in the NMR tube and sealed. The shift of  $^1\text{H}$  NMR signal of HMDS was then measured. Effective magnetic moment ( $\mu_{\text{eff}}$ ) of **2** was estimated in a similar way as described above.

**Magnetic Susceptibility Measurement.** Magnetic susceptibility of **1** over a temperature range 4–300K was measured in a Physical Property Measurement System (PPMS) from Cryogenic Limited, UK. During the measurement, a 2 T magnetic field was applied. Diamagnetic correction from the sample as well as sample holder was applied during analysis of the data.

**Mass Spectrometry.** ESI-mass spectra were recorded in a Bruker Micro-TOF QII spectrometer. GC-mass spectra of the organic compounds were measured in an Agilent 7890B GC system fitted with a FID detector and Agilent 5977B GC/MSD mass detector.

**Infrared Spectroscopy.** Fourier transform infrared spectrum of complex **1** was measured on KBr pellets in a Nicolet protégé 460 ESP instrument.

**CHN analysis.** Elemental analysis of complex **1** was performed in a PerkinElmer's 2400 Series II CHNS/O System.

**Electrochemistry.** Cyclic voltammetry (CV) and differential pulse voltammograms (DPV) were measured in a CH Instrument (CHI 760E, CH Instrument, USA) using glassy carbon (ID: 3 mm diameter) as working electrode, Pt wire as counter electrode, and Ag/AgCl (in saturated KCl) as the reference electrode. A 0.6 mM solution of **1** in acetonitrile containing 60 mM tetrabutylammonium hexafluorophosphate as counter electrolyte was used. All the electrochemical measurements were performed under nitrogen atmosphere using deoxygenated acetonitrile.

**EPR Spectroscopy.** EPR spectra of the complexes were recorded in a Bruker EPR spectrometer (Biospin, EMXmicro A200).

In a typical experiment, a 400  $\mu\text{L}$  of a 0.5 mM solution of complex **1** in acetonitrile was introduced in an EPR tube inside a nitrogen filled glovebox. The tube was taken outside of the glovebox, frozen in liquid nitrogen and inserted in the cavity of the EPR instrument precooled at 100K. Once the measurement was over, the sample tube was warmed to approx.  $-25\text{ }^\circ\text{C}$  in an acetone bath, followed by 30  $\mu\text{L}$  of a 6.6 mM solution of TBAH (one equiv.) was inserted into the EPR tube and the reaction solution was homogenised by bubbling nitrogen gas into the solution. The EPR tube was further reinserted in the cavity of the instrument and the measurement was conducted at 100K.

**UV-Vis Spectroscopy.** UV-Vis spectra were collected in an Agilent 8454 Diode array spectrophotometer fitted with a low temperature cryostat (UNISOKU, Japan). In a typical experiment, a 3 mL of a 0.25 mM solution of complex **1** in acetonitrile was taken in a 1 cm pathlength cuvette inside the glovebox. Then, the cuvette was taken out from the glovebox and placed inside the cryostat where the temperature of holder fixed at  $-25\text{ }^{\circ}\text{C}$  (or  $-45\text{ }^{\circ}\text{C}$ ). The temperature of the reaction solution was allowed to equilibrate for 5 minutes. A 50  $\mu\text{L}$  solution of TBAH (15 mM) in acetonitrile was introduced in the cuvette and single spectra of the reaction solution was measured continuously while stirring the reaction solution. The formation of the complex **2** was monitored at 470 and 680 nm. After complete formation of the intermediate (**2**), desired amount of substrate (20–100  $\mu\text{L}$ , 4-X-2,6-di-*tert*-butylphenol or Gomberg's dimer) was introduced into the reaction solution and reaction was monitored at 470 nm by UV-Vis spectroscopy under pseudo-first-order or second order reaction condition. The second order rate constants were obtained plotting  $k_{\text{obs}}$  vs [substrate] or  $(A_0 - A)/(C_0)(A - A_{\infty})$  vs. time (s) for pseudo-first-order or second-order reactions, respectively.

The  $\text{PK}_a$  value of **2** was determined by spectrophotometric titration using pyrrolidine as a base. We used a similar experimental procedure as described in the literature.<sup>6</sup>

### **X Ray structure determination.**

Crystals of complex **1** suitable for single-crystal X-ray diffraction studies were selected from the mother liquor and immersed in Paratone oil followed by mounting on a nylon loop under a 100 K nitrogen cold stream. Data collections were performed on a Bruker D8 VENTURE Microfocus diffractometer equipped with PHOTON II Detector, with Mo  $\text{K}\alpha$  radiation ( $\lambda = 0.71073\text{ \AA}$ ), controlled by the APEX III (v2017.3–0) software package. The raw data were integrated and corrected for Lorentz and polarization effects with the aid of the Bruker APEX III program suite.<sup>7</sup> Absorption corrections were performed by using SADABS. Structures were solved by the intrinsic phasing method and refined against all data in the reported  $2\theta$  ranges by full-matrix least squares method based on F2 using the SHELXL program suite<sup>8</sup> with all observed reflections. Hydrogen atoms at idealized positions were included in final refinements. The non-hydrogen atoms were treated anisotropically. Diagrams for the complexes were prepared using ORTEP.<sup>9</sup> and Mercury software.<sup>10</sup> Crystallographic data of complex **1** is given in Table S1 and bond parameters are mentioned in Table S2. CCDC number 2018882 contain crystallographic data of complex **1**.

**Table S1.** Summary of X-ray crystallographic data of complex **1**• 2H<sub>2</sub>O.

	<b>1</b>
Empirical formula	C <sub>22</sub> H <sub>45</sub> FeN <sub>4</sub> O <sub>7</sub>
Formula weight	533.47
Crystal system	Monoclinic
Space group	<i>P2(1)/c</i>
<i>a</i> (Å)	13.571(4)
<i>b</i> (Å)	11.046(4)
<i>c</i> (Å)	19.406(6)
$\alpha$ (deg.)	90
$\beta$ (deg.)	102.992(11)
$\gamma$ (deg.)	90
Volume (Å <sup>3</sup> )	2834.6(17)
<i>Z</i>	4
<i>D</i> <sub>calcd.</sub> (mg/m <sup>3</sup> )	1.250
$\mu$ Mo-K $\alpha$ (mm <sup>-1</sup> )	0.575
<i>F</i> (000)	1148
$\theta$ range (deg.)	2.771–33.535
Reflections collected	38789
Reflections unique	10231
<i>R</i> (int)	0.0783
Data ( <i>I</i> >2 $\sigma$ ( <i>I</i> ))	7340
Parameters refined	339
Goodness-of-fit on <i>F</i> <sup>2</sup>	1.067
<i>R</i> 1 [ <i>I</i> >2 $\sigma$ ( <i>I</i> )]	0.0617
<i>wR</i> 2	0.1573

**Table S2.** Important bond length (Å) and bond angles (°) for complex **1**.

Fe(1)–O(1)	1.9093(17)	O(1)–Fe(1)–N(1)	109.61(8)
Fe(1)–O(2)	1.9273(17)	O(3)–Fe(1)–O(2)	103.64(7)
Fe(1)–O(3)	1.9222(16)	O(3)–Fe(1)–N(2)	80.71(7)
Fe(1)–N(1)	2.0684(18)	O(3)–Fe(1)–N(1)	137.84(7)
Fe(1)–N(2)	2.0724(18)	O(2)–Fe(1)–N(2)	147.36(7)
O(1)–Fe(1)–O(3)	108.77(7)	O(2)–Fe(1)–N(1)	80.20(7)
O(1)–Fe(1)–O(2)	108.24(8)	N(1)–Fe(1)–N(2)	75.80(7)
O(1)–Fe(1)–N(2)	100.52(7)		

## X-ray Absorption Spectroscopy

### 1. X-ray Absorption Near Edge (XANES) and Extended X-ray Absorption Fine Structure (EXAFS) Measurements

X-ray absorption spectra on complexes **[1]** and **[2]** were carried out at the Petra P64 beamline<sup>11</sup> (Hamburg, Germany) at electron energy 7.1 KeV and average current 100 mA. The radiation was monochromatized by a Si(111) crystal monochromator. The intensity of the X-ray was monitored by three ion chambers ( $I_0$ ,  $I_1$  and  $I_2$ ) filled with 70% nitrogen and 30% helium and placed before the sample ( $I_0$ ) and after the sample ( $I_1$  and  $I_2$ ). A Fe metal foil was placed between the  $I_1$  and  $I_2$  and its absorption recorded with each scan for energy calibration. Plastic (PEEK) EXAFS sample holders (inner dimensions of 12 mm x 3 mm x 3mm) filled with the frozen solutions of **[1]** and **[2]** were inserted into a pre-cooled (20 K) cryostat and kept in a He atmosphere at ambient pressure. The XAS data was in this case recorded as fluorescence excitation spectra using a 4-element silicon drift detector. The Fe XAS energy was calibrated by the first maximum of the second derivative of the Fe metal XANES spectrum. A total of 8-10 scans were collected for complexes **[1]** and **[2]**. In order to reduce the risk of sample damage by X-ray radiation, no more than 2 scans were taken at each sample position in any conditions. No radiation damage was observed to any of the two samples scan after scan.

### 2. EXAFS Data Analysis

Athena software<sup>12</sup> was used for data processing. The energy scale for each scan is normalized using the iron metal standard and scans made for the same samples were added. Data in energy space are pre-edge corrected, normalized, and background corrected. The processed data are next converted to the photoelectron wave vector ( $k$ ) space and weighted by  $k^2$ . The electron wave number is defined as  $k = [2m(E - E_0)/\hbar^2]^{1/2}$ ,  $E_0$  is the energy origin or the threshold energy.  $k$ -space data were truncated near the zero crossings ( $k = 2$  to  $14.107 \text{ \AA}^{-1}$ ) in Fe EXAFS before Fourier transformation. The  $k$ -space data were then transferred into the Artemis Software for curve fitting. In order to fit the data, the Fourier peaks are isolated separately, grouped together, or the entire (unfiltered) spectrum was used. The individual Fourier peaks were isolated by applying a Hanning window to the first and last 15% of the chosen range, leaving the middle 70% untouched. Curve fitting is performed using *ab initio*-calculated phases and amplitudes from the FEFF8<sup>13</sup> program and *ab initio*-calculated phases and amplitudes are used in the EXAFS equation<sup>14</sup>

$$\chi(k) = S_0^2 \sum_j \frac{N_j}{kR_j^2} f_{\text{eff}_j}(\pi, k, R_j) e^{-2\sigma_j^2 k^2} e^{\frac{-2R_j}{\lambda_j(k)}} \sin(2kR_j + \phi_j(k)) \quad (\text{S1})$$

where  $N_j$  is the number of atoms in the  $j^{\text{th}}$  shell;  $R_j$  the mean distance between the absorbing atom and the atoms in the  $j^{\text{th}}$  shell;  $f_{\text{eff}_j}(\pi, k, R_j)$  is the *ab initio* amplitude function for shell  $j$ , and the Debye-Waller term  $e^{-2\sigma_j^2 k^2}$  accounts for damping due to static and thermal disorder in absorber-backscatterer distances. The mean free path term  $e^{\frac{-2R_j}{\lambda_j(k)}}$  reflects losses due to inelastic scattering, where  $\lambda_j(k)$  is the electron mean free path. The oscillations in the EXAFS spectrum are reflected in the sinusoidal term  $\sin(2kR_j + \phi_j(k))$ , where  $\phi_j(k)$  is the *ab initio* phase function for shell  $j$ . This sinusoidal term shows the direct relation between the frequency of the EXAFS oscillations in k-space and the absorber-back scatterer distance.  $S_0^2$  is an amplitude reduction factor.

The EXAFS equation (Eq. S1) is used to fit the experimental Fourier isolated data (in q-space) as well as unfiltered data (in k-space) and Fourier transformed data (in R-space) using  $N$ ,  $S_0^2$ ,  $E_0$ ,  $R$ , and  $\sigma^2$  as variable parameters.  $N$  refers to the number of coordination atoms surrounding Fe for each shell. The quality of fit is evaluated by R-factor and the reduced  $\chi^2$  value. The deviation in  $E_0$  was required to be less than or equal to 10 eV. An R-factor less than 2% denotes that the fit is good enough whereas an R-factor between 2 and 5% denotes that the fit is correct within a consistently broad model<sup>14</sup>. The reduced  $\chi^2$  value is used to compare fits as more absorber-backscatter shells are included to fit the data. A smaller reduced  $\chi^2$  value indicates a better fit. Similar results were obtained from fits done in k, q, and R-spaces.

**Table S3.** EXAFS Fits parameters

Complex	Fit	Region	Shell, N	R, Å	$E_0$	ss. <sup>2</sup> (10 <sup>-3</sup> )	R-factor	Reduced Chi-square
<b>1</b>	1	I	Fe-N/O, 5	1.95	-1.0	9.2	0.0442	8664
	2	I	Fe-O, 3 Fe-N, 2	1.88 2.03	-2.7	2.5	0.0035	1227
	<b>3</b>	<b>I,II</b>	<b>Fe-O,3 Fe-N,2 Fe-C,6 Fe-C- N/O,16</b>	<b>1.88 (1) 2.04 (1) 2.90 (2) 3.17 (1)</b>	<b>-0.77 (1.3)</b>	<b>3.7 (1.3) 1.3 (0.8) 6.8 (2.0) 1.4 (1.2)</b>	<b>0.0039</b>	<b>813</b>
Ligand Oxidized <b>2</b>	4	I	Fe-N/O,5	1.94	-0.9	14.6	0.0217	4911
	5	I	Fe-O,3 Fe-N,2	1.91 2.10	1.7	6.7 4.4	0.0163	6539
	<b>6</b>	<b>I,II</b>	<b>Fe-O,3 Fe-N,2 Fe-C,6 Fe-C- N/O,16</b>	<b>1.89 (2) 2.09 (2) 2.87 (2) 3.12 (2)</b>	<b>0.72 (2.1)</b>	<b>6.7 (1.7) 4.3 (2.3) 6.0 (1.4) 7.1 (5.0)</b>	<b>0.0055</b>	<b>1176</b>

\* The amplitude reduction factor  $S_0^2$  was fixed to 1. Region I refers to the EXAFS spectra region between apparent distances 1.1-2.1 Å whereas Regions I and II refer to that between 1.1-3 Å. Fits 3 and 6 for the entire spectrum are highlighted in bold in table S3 above. The numbers in brackets refers to the error bars which range in the order of 0.02-0.03 Å in the extracted bond distances.

**Table S4.** A comparison of the bond lengths (Å) of **1** obtained from XRD and EXAFS measurements.

<b>Bonds</b>	<b>X-ray Structure</b>	<b>EXAFS</b>
Fe(1)–O(1)	1.9093(17)	1.88(1)
Fe(1)–O(2)	1.9273(17)	1.88(1)
Fe(1)–O(3)	1.9222(16)	1.88(1)
Fe(1)–N(1)	2.0684(18)	2.04(1)
Fe(1)–N(2)	2.0724(18)	2.04(1)

### Pre-edge fit parameters for Complexes' [1] and [2]

The pre-edge area peaks were carried out with an error function and a pseudo-voight function in the Athena<sup>12</sup> software using the peak-fitting function. The formulas for the error(erf) and pseudo-voight function employed for the pre-edge fits are shown in equations S2 and S3.

$$\text{Error function: } A \left[ \text{erf} \left( \frac{e - E_0}{w} \right) + 1 \right] \quad (\text{Eq.S2})$$

The pseudo-voight profile is given by

$$V(x; \sigma, \gamma) \equiv \int_{-\infty}^{\infty} G(x'; \sigma) L(x - x'; \gamma) dx'; \quad (\text{Eq.S3})$$

Where  $x$  is the shift from the line centre,

$$G(x; \sigma) \text{ is the centred Gaussian profile where } G(x; \sigma) \equiv \frac{e^{-x^2/2\sigma^2}}{\sigma\sqrt{2\pi}}, \quad (\text{Eq.S4})$$

$$\text{and } L(x; \gamma) \text{ is the centred Gaussian profile, } L(x; \gamma) \equiv \frac{\gamma}{\pi(x^2 + \gamma^2)}, \quad (\text{Eq.S5})$$

The parameters  $A$ ,  $E_0$ ,  $w$ ,  $\sigma$  and  $\gamma$  for complexes **[1]** and **[2]** are tabulated below.

**Table S5:** Summary of parameters employed for the pre-edge fits of complexes **[1]** and **[2]**

<b>Pseudo-Voight Function</b>	$E_0$ (Centroid, eV)	$\sigma$	$\gamma$	<b>AREA (units)</b>
Complex <b>[1]</b>	7113.97	2.038	0.385	19.3
Complex <b>[2]</b>	7113.71	2.119	0.385	16.1
<b>Erf function</b>	$E_0$ (Centroid, eV)	$w$ (Width)	$A$ (Amplitude)	
Complex <b>[1]</b>	7139.00	16.286	0.592	



Complex [2]	7139.00	14.720	1.113
-------------	---------	--------	-------

The pre-edge area peaks fitting were further re-carried out in the Fityk<sup>15</sup> software and as previously demonstrated<sup>16</sup>, and the same pre-edge peak areas of 19.3 and 16.1 units were obtained for Complexes' [1] and [2] respectively thus confirming the fit procedure employed in the Athena<sup>12</sup> software.

**Complex's [1] DFT Calculations.** The DFT optimization calculations were performed using the ORCA (Version 4.2.0) program package developed by Neese<sup>17</sup> and co-workers. The calculations were carried out using a variety of functionals and basis sets. Calculation (1) was carried out using the B3LYP<sup>18, 19</sup> exchange-correlation functional in combination with the triple zeta valence polarization function (def2-TZVP)<sup>20</sup>, and the atom-pairwise dispersion correction with the Becke-Johnson damping scheme (D3BJ)<sup>21, 22</sup>. Calculation (2) was furthermore optimized at the BP-86 level<sup>23, 24</sup> with the def2-TZVP<sup>20</sup> basis set, and the atom-pairwise dispersion correction D3BJ<sup>21, 22</sup>. Calculation (3) was repeated at the BLYP<sup>25</sup> level using the same basis and dispersion correction as calculations (1) and (2).

Calculation (4) was carried out using the Perdew-Burke-Erzerhoff GGA function<sup>24</sup> with the SVP polarized valence double-zeta basis set, and same dispersion corrections as calculations (1)-(3). Calculation (5) was carried out using the BP86<sup>23, 24</sup> exchange-correlation functional using the 6-31+G\* basis set<sup>26-30</sup> as previously reported<sup>16</sup> and the atom-pairwise dispersion correction D3BJ<sup>21, 22</sup>. Calculation (6) was finally carried out at the B3LYP<sup>18, 19</sup> functional using the same basis set and dispersion correction as calculation (5).

The conductor-like polarizable continuum model (CPCM)<sup>31</sup> was applied in all calculation(1)-(6) to model the acetonitrile solvent. The RI<sup>32</sup> approximations were on the one hand used to accelerate Coulomb and exchange integrals for calculations (2), (4) and (5). On the other hand, the RIJCOSX<sup>32</sup> approximations were used to accelerate Coulomb and exchange integrals for calculations (1) and (6). The default GRID settings were further used for the self-consistent field iterations and for the final energy evaluation. The calculated structures were confirmed to be minima based on a check of the energies and the absence of imaginary frequencies from frequency calculations carried out on the optimized geometries.

**Table S6:** DFT calculations using various approaches and basis sets for Complex [1]

	XRD	B3LYP- def2- TZVP, D3BJ (1)	BP86 def2- TZVP, D3BJ (2)	BLYP- def2- TZVP, D3BJ (3)	PBE- SVP D3BJ (4)	BP86 6-31+G* D3BJ (5)	B3LYP 6-31+G* D3BJ (6)
Fe-O(1)	1.909	1.992	1.993	2.012	1.987	1.997	1.980
Fe-O(2)	1.922	1.908	1.902	1.918	1.898	1.903	1.895
Fe-O(3)	1.927	1.893	1.890	1.905	1.902	1.894	1.904
Fe-N(1)	2.072	1.916	1.908	1.926	1.923	1.910	1.919
Fe-N(2)	2.068	1.918	1.912	1.931	1.920	1.912	1.924
O(1)-Fe- O(3)	108.24	104.41	101.68	101.90	103.87	101.95	102.25
O(1)-Fe- O(2)	108.77	105.29	104.68	104.56	103.42	104.11	103.10
O(1)-Fe- N(2)	109.61	104.43	103.78	104.08	103.20	103.70	103.06
O(1)-Fe-	100.52	101.21	103.56	103.44	104.03	103.74	104.59

N(1)							
O(3)-Fe-O(2)	103.64	96.62	96.61	96.98	97.05	96.54	97.92
O(3)-Fe-N(2)	80.20	84.16	84.33	84.18	84.09	84.26	83.56
O(3)-Fe-N(1)	147.36	153.30	153.63	153.51	150.98	153.26	151.93
O(2)-Fe-N(2)	137.84	149.05	150.69	150.43	152.24	151.36	152.84
N(1)-Fe-N(2)	75.80	82.33	82.40	82.28	81.92	82.61	82.53

### Synthesis.

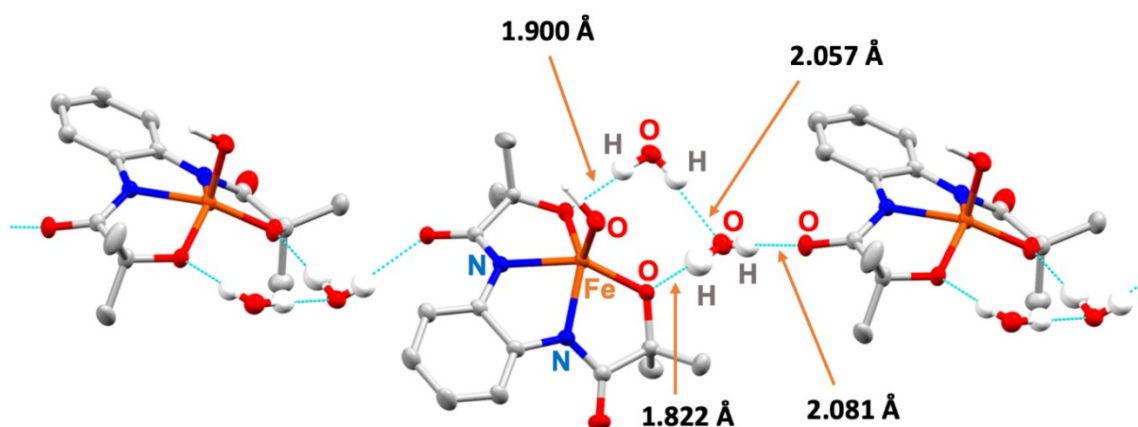
**Complex 1.** The H<sub>4</sub>L (0.11 g, 0.4 mmol) was taken in a reaction bath inside the glovebox, and 2 mL of methanol was added to it. To the stirring ligand solution, 0.65 g of Me<sub>4</sub>NOH (25 % solution in methanol; 1.8 mmol, 4.5 equiv.) was added and allowed to stir for 2 minutes. A methanolic solution (3 mL) of Fe(ClO<sub>4</sub>)<sub>3</sub> • H<sub>2</sub>O (0.14 g, 0.4 mmol) was slowly added to the stirring reaction solution and allowed to stir at room temperature for 1 h. Precipitation of tetramethylammonium perchlorate was observed while stirring. The reaction solution was filtered and the methanolic solution was dried under reduced pressure to dryness. Acetonitrile (3 mL) was added to the reaction mixture to dissolve the residue. Excess diethyl ether was added to the reaction mixture and stir the reaction mixture for a while. The mixture was kept at –20 °C inside the refrigerator for overnight. Precipitation of a yellowish-brown solid takes place. The solid compound was separated and dried under vacuum. Single crystals suitable for X-ray diffraction quality was obtained upon diffusing diethyl ether into an acetonitrile solution of the complex at room temperature. Yield: 39 % (0.08 g). Anal. Calcd for 1•H<sub>2</sub>O (C<sub>22</sub>H<sub>41</sub>FeN<sub>4</sub>O<sub>5</sub>• H<sub>2</sub>O, 515.45 g/mol): C, 51.26; H, 8.41; N, 10.87. Found: C, 51.28; H, 8.77; N, 10.74. IR (KBr, cm<sup>-1</sup>): 3415 (br), 3017 (m), 2967 (m), 2927 (m), 1658 (m), 1592 (m), 1542 (vs), 1487 (vs), 1451 (m), 1362 (s), 1398 (s), 1242 (m), 1165 (m), 976 (m), 950 (vs), 770 (m), 652 (m), 602 (m), 560 (m). ESI-MS (negative ion mode, acetonitrile): *m/z* = 332.32 ([LFe]<sup>-</sup>).

### Product Analysis.

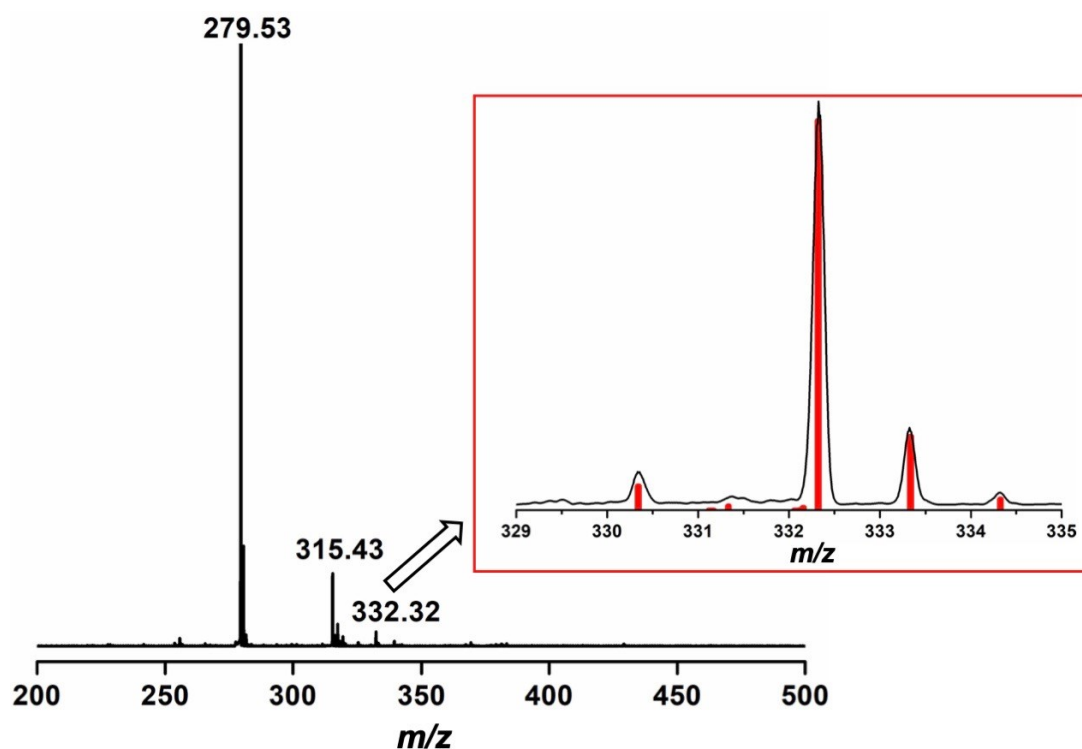
**Reaction of 2 with 2,6-di-*tert*-butyl-4-methoxyphenol.** A 3 mL of a 0.5 mM solution of complex 1 was taken in a 10 mL reaction bath fitted with a septum and stir bar under nitrogen environment. The reaction bath was cooled at –25 °C in an acetone-liq. N<sub>2</sub> bath. To the stirring reaction solution one equiv. of TBAH was added and stirred for 10 minutes. After the complete formation of the intermediate 2, one equiv. of 2,6-di-*tert*-butyl-4-methoxyphenol was introduced to the reaction solution through a gas-tight syringe under nitrogen atmosphere and the reaction solution was stirred for 30 minutes at –25 °C. Once the reaction is completed, the reaction solution was warmed to room temperature, passed through a short silica gel column, and analysed through GC-mass.

**Reaction of 2 with Gomberg's Dimer.** In a cuvette, 500 μL of a 0.5 mM solution of complex 1 in dry acetonitrile was introduced inside the glovebox and sealed with a septum. The cuvette was placed at –40 °C in the UNISOKU cryostat outside the glovebox. One equiv. of TBAH

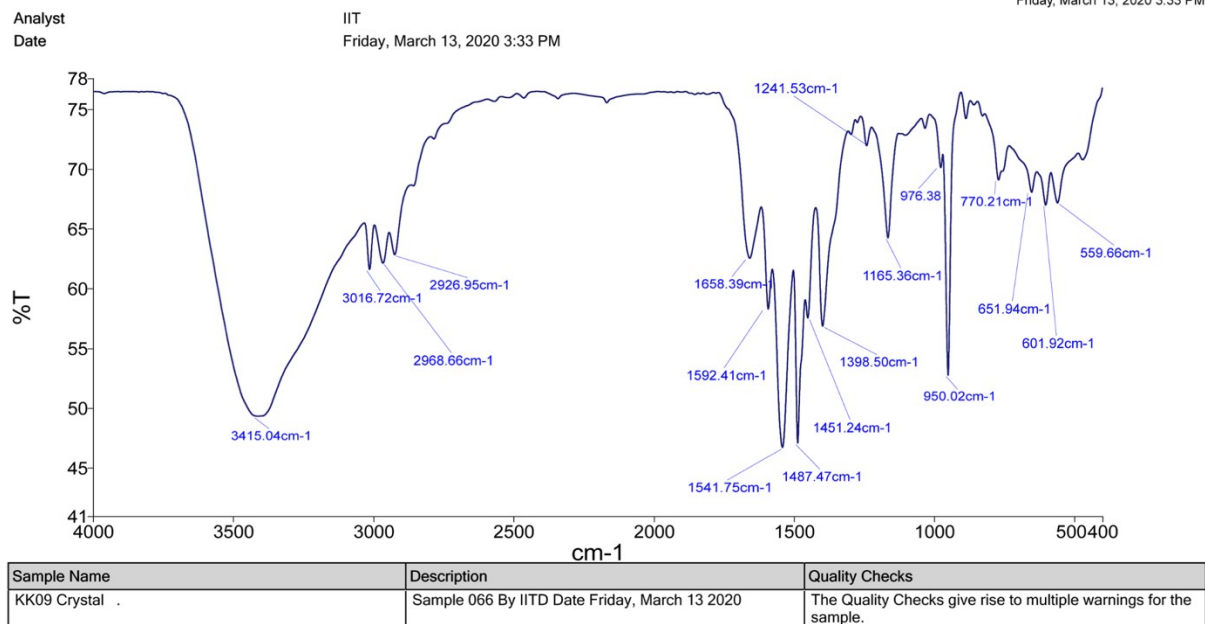
(30  $\mu\text{L}$  of a 8.33 mM solution) was introduced inside the cuvette and stirred at  $-40\text{ }^\circ\text{C}$  for 10 minutes. Then, 10  $\mu\text{L}$  of  $\text{H}_2\text{O}^{18}$  was carefully introduced into the reaction solution and allowed to stir at  $-40\text{ }^\circ\text{C}$  for 1 h. Gomberg's dimer (5 equiv.) was then introduced into the reaction solution and allowed to stir for 2h at  $-40\text{ }^\circ\text{C}$ . Then, the cuvette was warmed to room temperature, and the reaction solution was passed through a short silica gel column to separate iron. The reaction solution was then analysed by GC-mass and ESI-mass spectrometry.



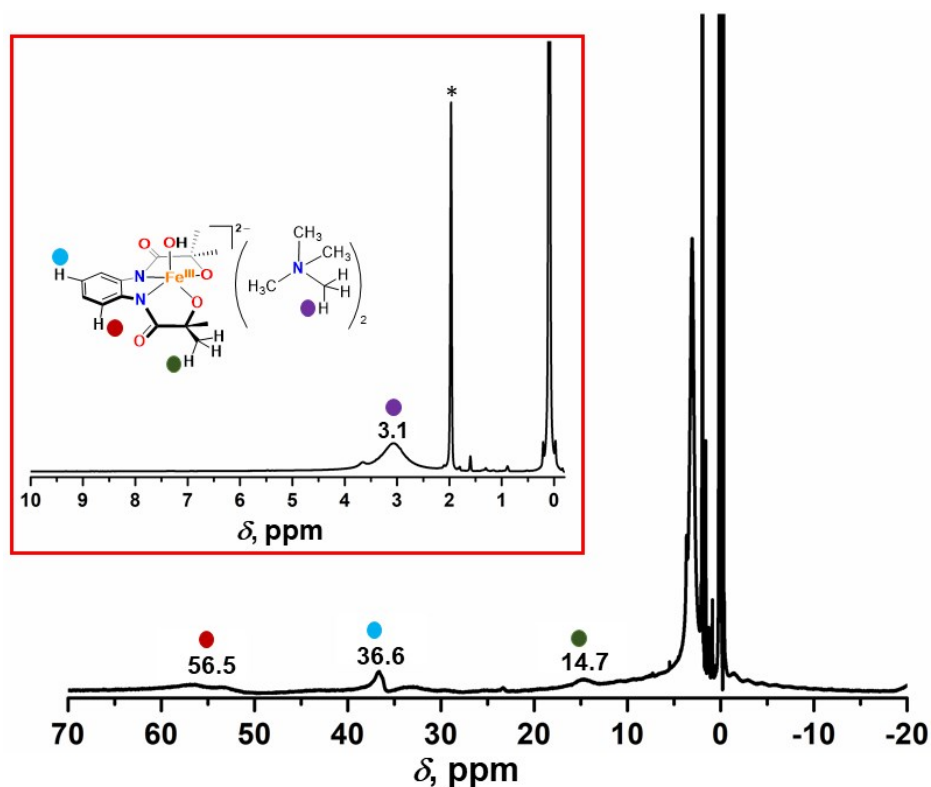
**Figure S1.** Hydrogen bonding interactions observed in the solid-state structure of complex **1**. All of the hydrogen atoms except those attached with hydroxide ion and water molecules have been omitted for clarity.



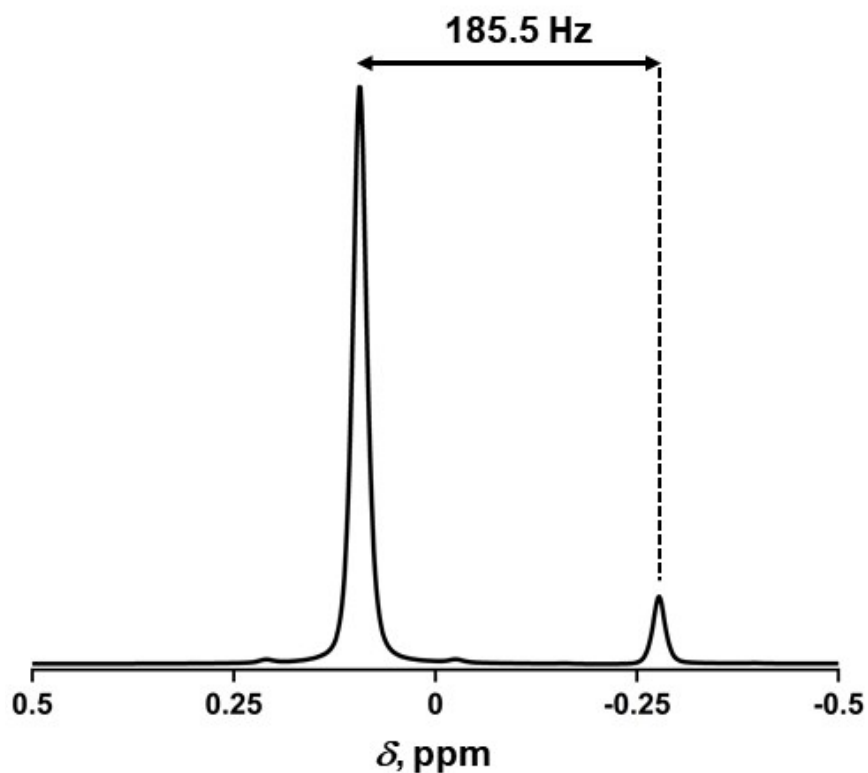
**Figure S2.** ESI mass spectrum of complex **1** in acetonitrile. Peak Assignments,  $m/z = 279.53$ , ( $[\text{H}_3\text{L}]^-$ ),  $m/z = 315.43$ , ( $[\text{L} + \text{Fe} - \text{OH}]^-$ ),  $m/z = 332.32$  ( $[(\text{L})\text{Fe}]^-$ ).



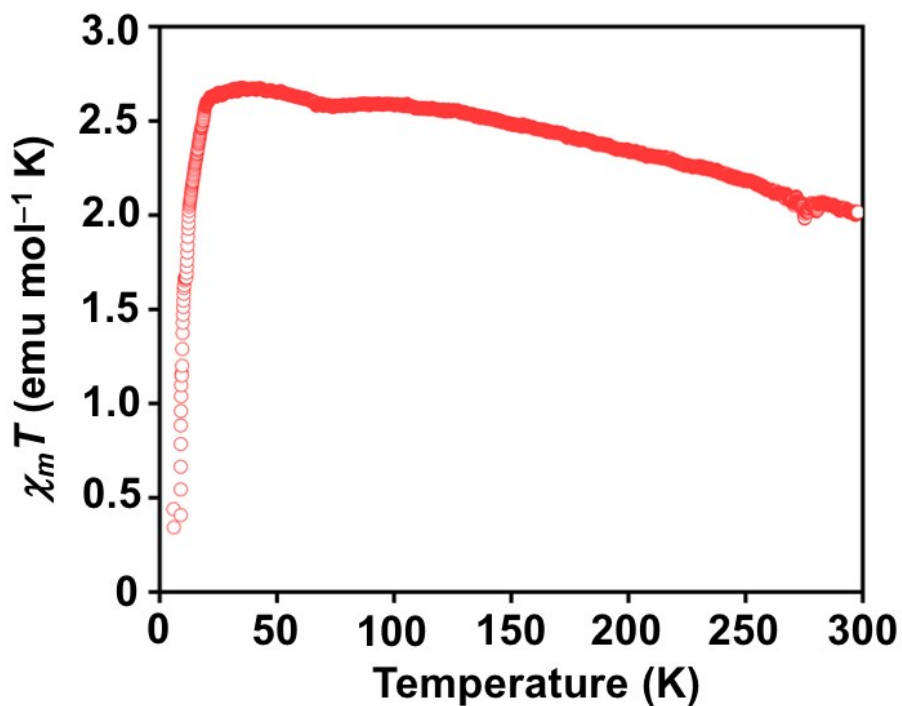
**Figure S3.** IR spectrum of complex **1**. The strong signal at  $3415\text{ cm}^{-1}$  is because of the presence of water molecules present in the crystal packing, which masks the O–H stretch coming from the OH group in the complex **1**.



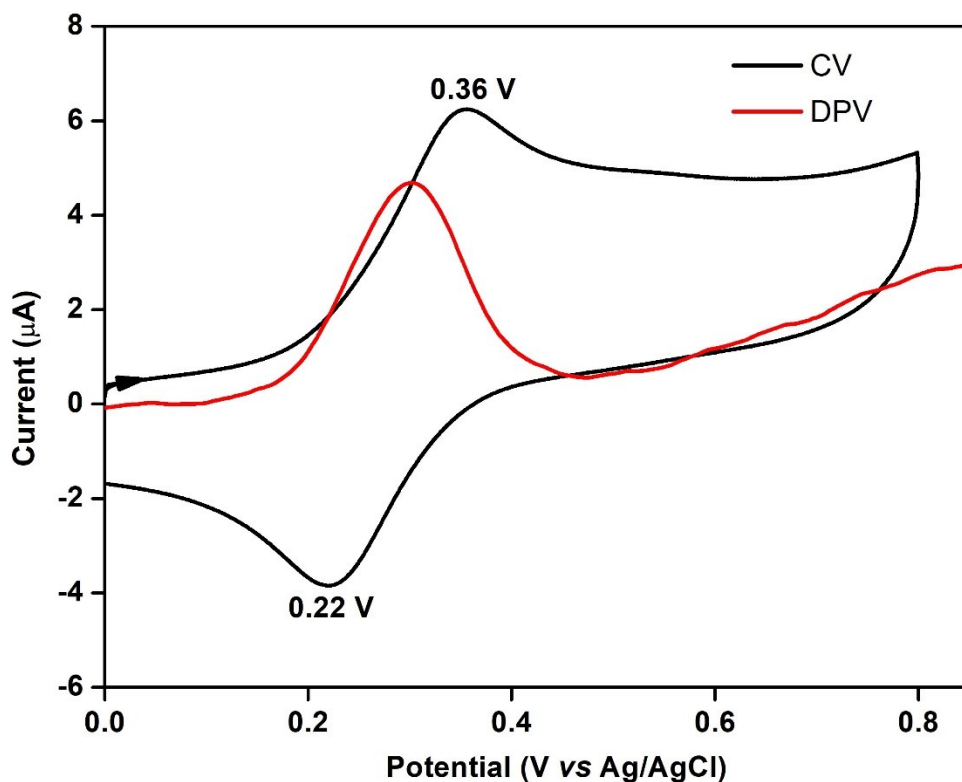
**Figure S4.**  $^1\text{H}$  NMR spectrum of complex **1** in  $\text{CD}_3\text{CN}$  at  $25\text{ }^\circ\text{C}$  in a 500 MHz NMR instrument.



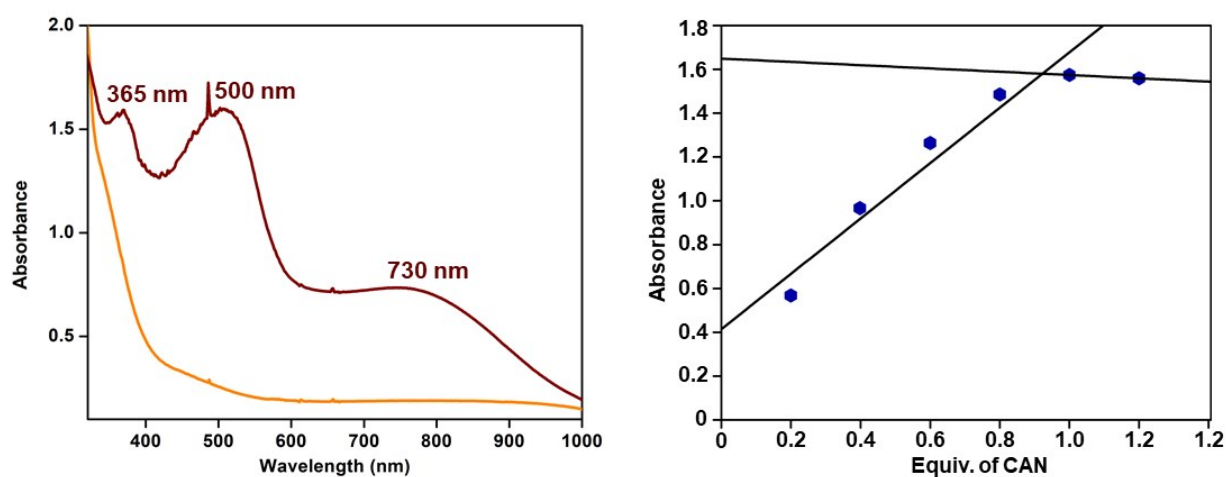
**Figure S5.** Shift of  $^1\text{H}$  NMR signal of hexamethyldisilazane in a 500 MHz NMR instrument for the estimation of magnetic moment of **1** (13 mM) in  $\text{CD}_3\text{CN}$  at 25  $^\circ\text{C}$ .



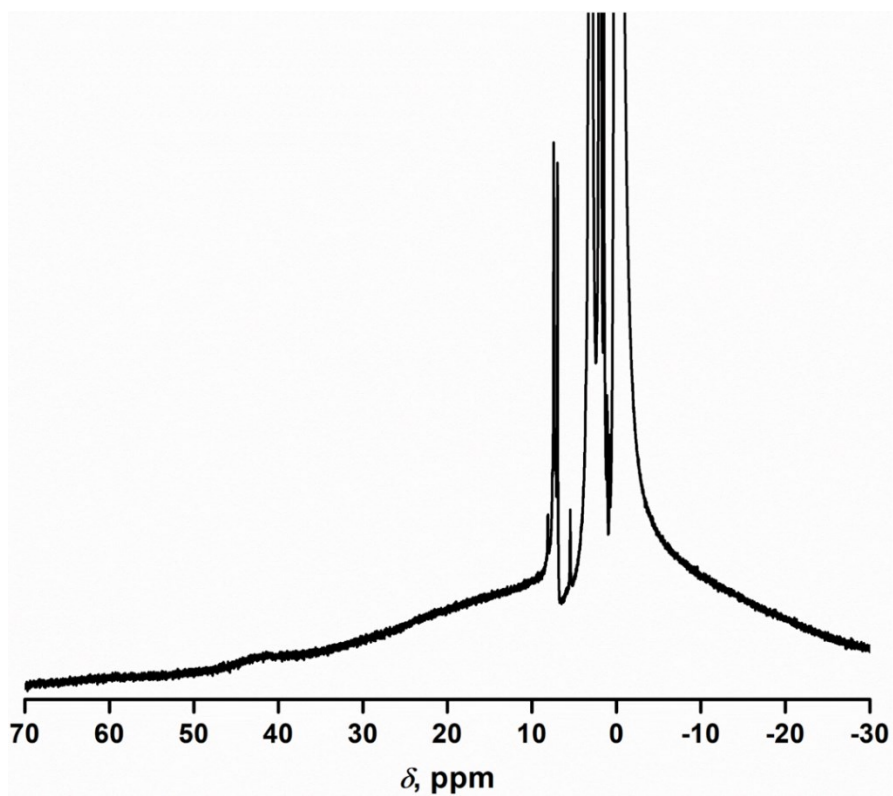
**Figure S6.** A plot of  $\chi_m T$  vs.  $T$  plot of **1** over a temperature range of 4–300 K. During the measurement, an applied magnetic field of 2 T was used.



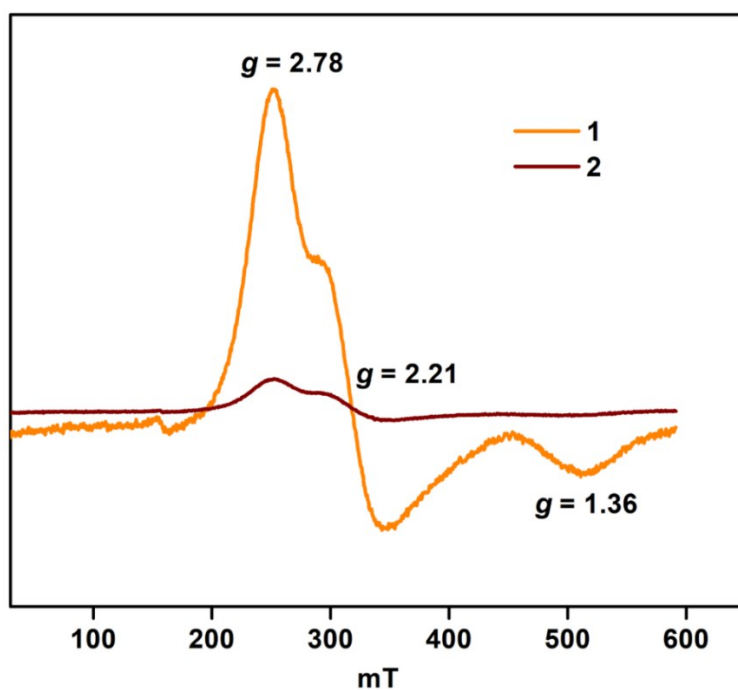
**Figure S7.** CV and DPV diagram of complex **1** (0.6 mM solution) in acetonitrile containing 0.06 M tetrabutylammonium hexafluorophosphate as counter electrolyte at 25 °C. A 3 mm glassy carbon working electrode, Pt wire counter electrode, and Ag/AgCl in saturated KCl was used as reference electrode during measurement. While CV measurement, 100 mV/s scan rate was used. The  $E_{1/2}$  value is  $-0.137$  V vs Fc/Fc<sup>+</sup> reference electrode.



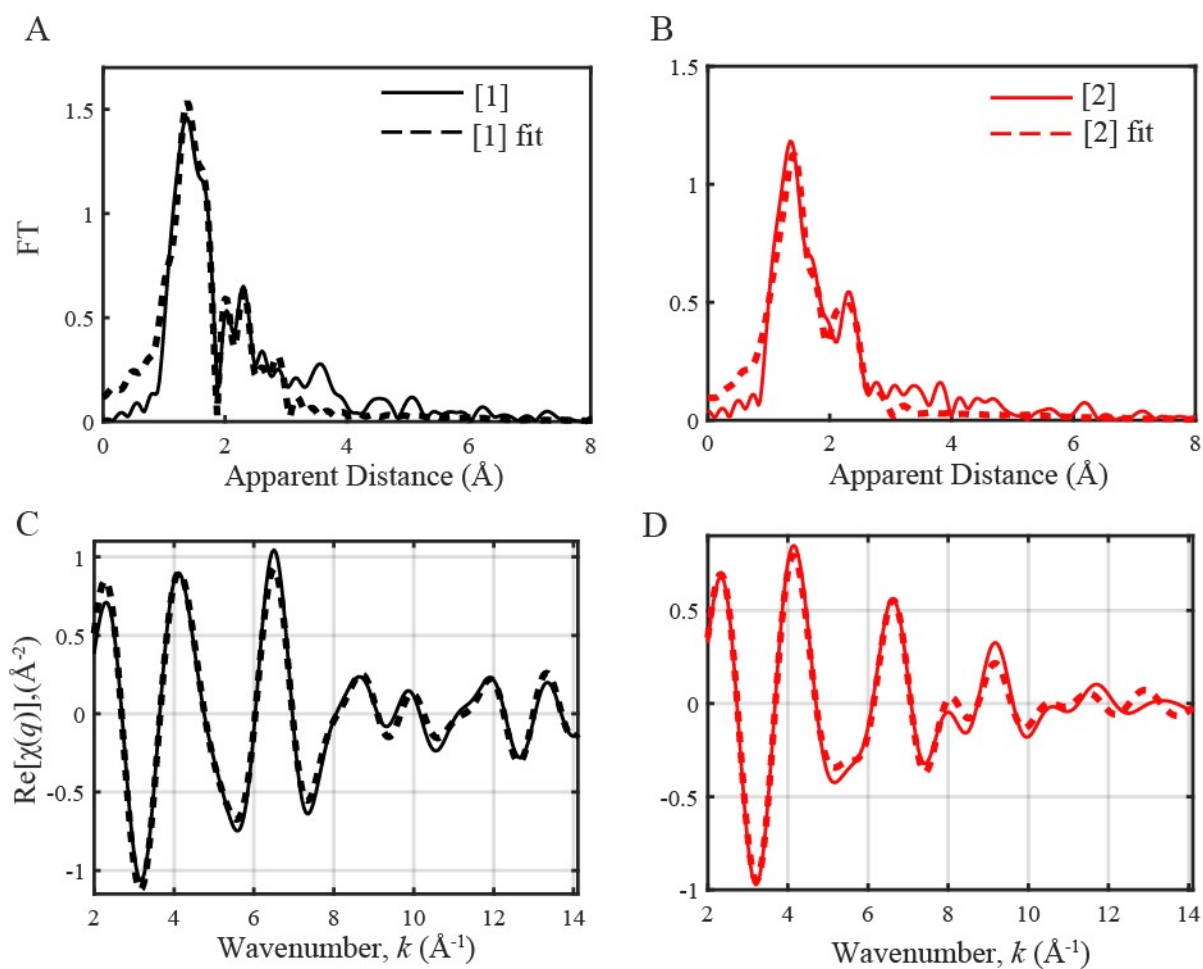
**Figure S8.** UV-Vis spectra of complex **1** (0.32 mM) and intermediate formed upon addition of 1 equiv. of ceric ammonium nitrate (CAN) to the solution of **1** in acetonitrile at  $-25$  °C.



**Figure S9.**  $^1\text{H}$  NMR spectrum of complex **2** in  $\text{CD}_3\text{CN}$  in a 500 MHz NMR instrument at  $-30^\circ\text{C}$ .

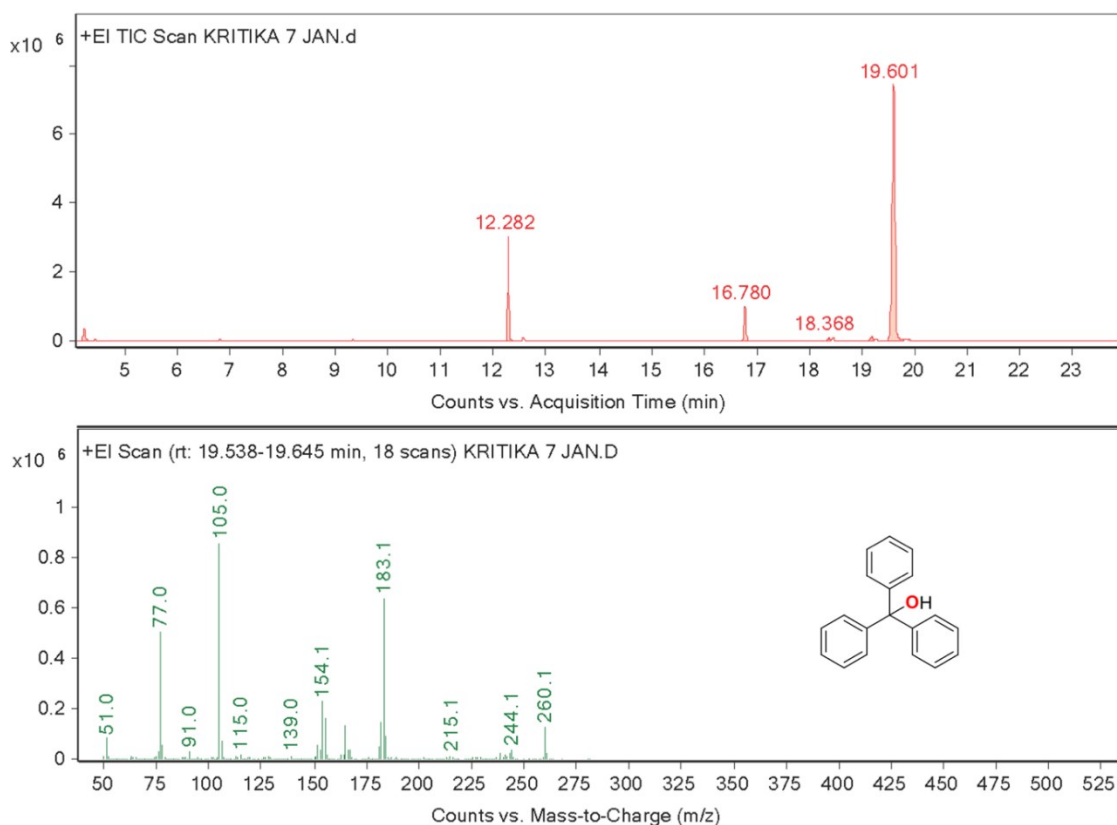


**Figure S10.** EPR spectrum of complex **1** and **2** in acetonitrile at 100 K. Quantification of EPR signal indicates that there is *ca.* 15% unreacted complex **1** in the reaction solution obtained upon addition of TBAH to **1** in acetonitrile.

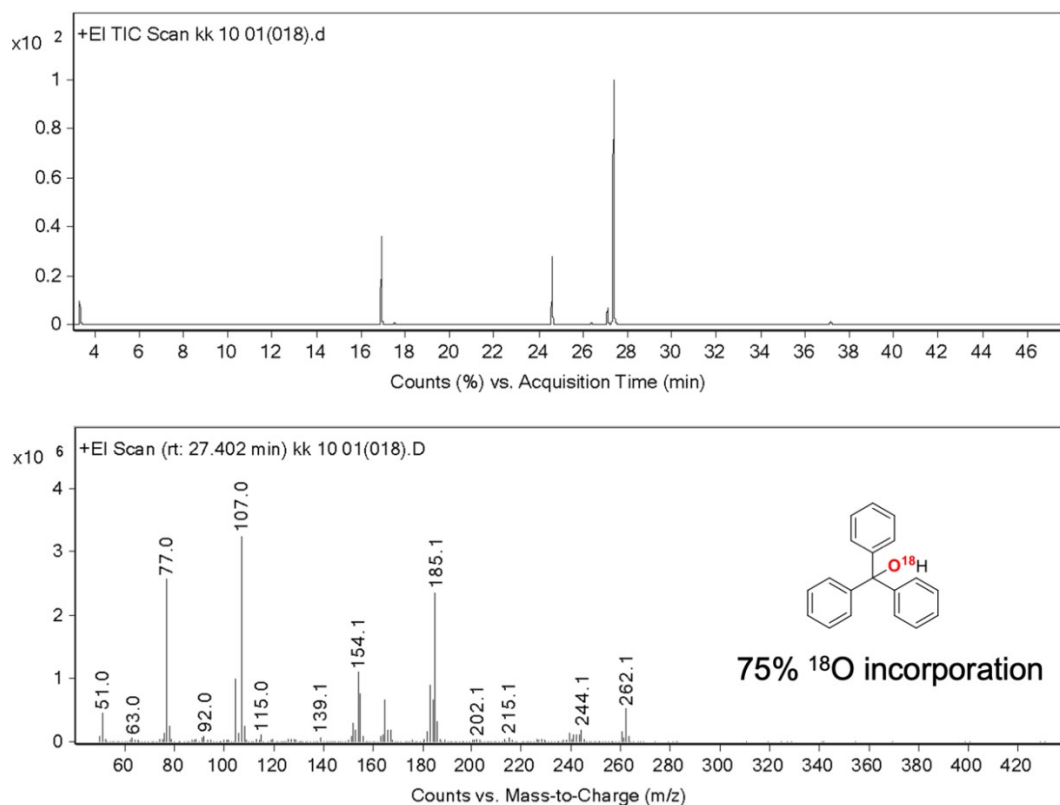


**Figure S11.** Fourier transforms of  $k^2$ -weighted Fe EXAFS for **A.** 5 mM Fe(III) complex **1** (solid black line) and its corresponding fit (Fit 3, Table S3), for **B.** the ligand oxidized product, complex **2**, generated with 1 equiv. of TBAH, (solid red line), and its corresponding fit (Fit 6, Table S3). Back Fourier transformed experimental (solid lines) and fitted (dashed lines)  $\text{Re}[\chi(q)]$  for **C.** Complex **1** (solid black line) and its corresponding fit (Fit 3, Table S3), for **D.** Complex **2** (solid red line) and its corresponding fit (Fit 6, Table S3).

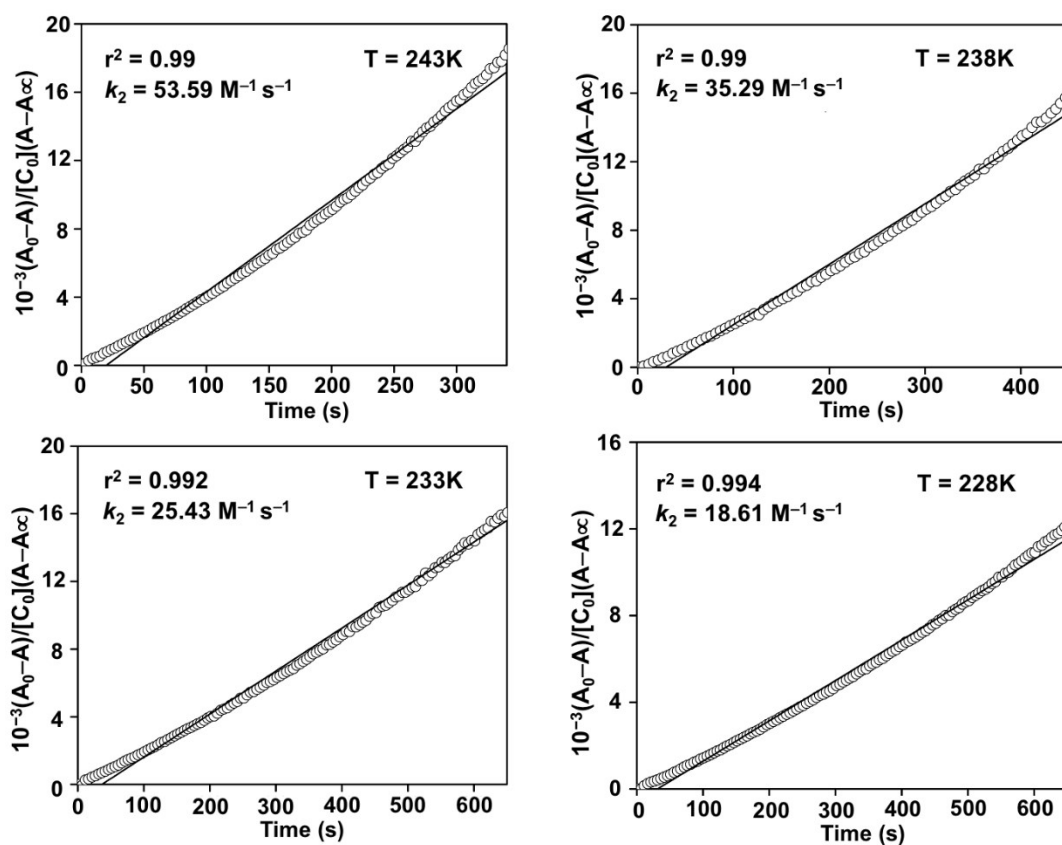




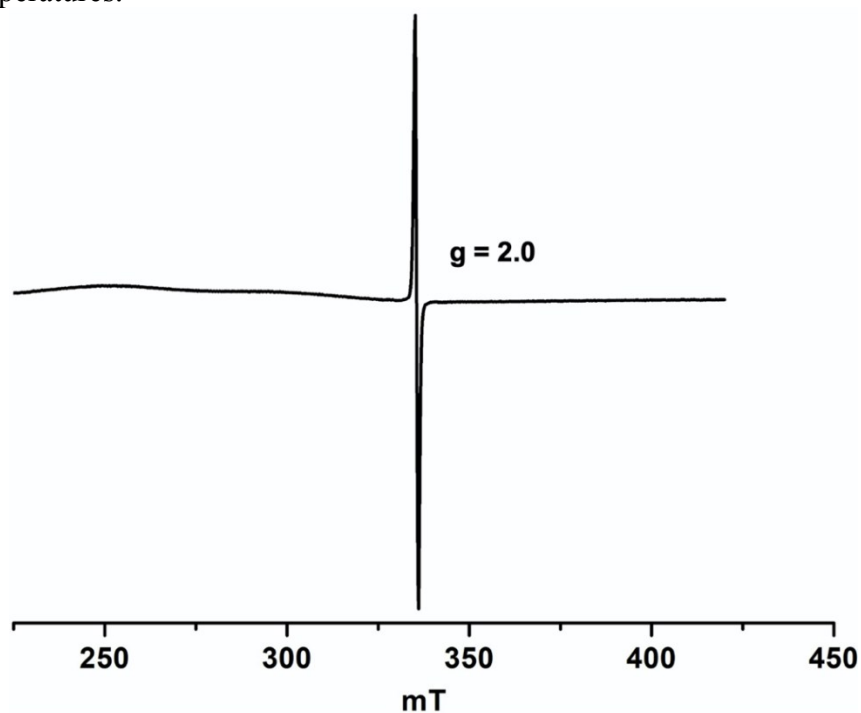
**Figure S12.** GC-mass spectrum of the reaction solution obtained upon reacting intermediate  $[(L^\bullet)\text{Fe}^{\text{III}}\text{OH}]^-$  (**2**) with Gomberg's dimer.



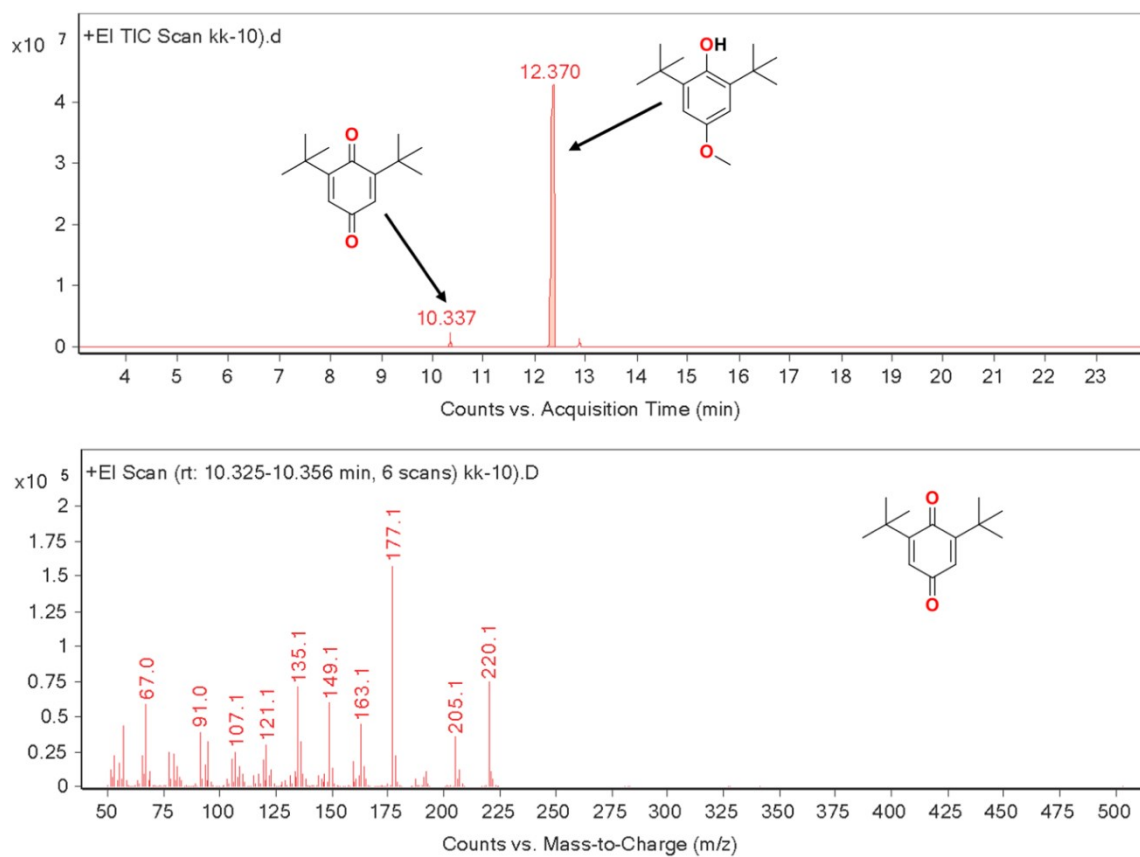
**Figure S13.** GC-mass spectrum of the reaction solution obtained upon reacting intermediate  $[(L^\bullet)\text{Fe}^{\text{III}}\text{O}^{18}\text{H}]^-$  with Gomberg's dimer.



**Figure S14.** Second-order fitting of the time trace at 470 nm at different temperatures of the reaction of **2** (0.32 mM) with 2,6-Di-*tert*-butyl-4-methoxyphenol (0.32 mM) in acetonitrile at different temperatures.



**Figure S15.** X-band EPR spectrum of the reaction mixture obtained upon addition of 0.5 mM of 2,6-Di-*tert*-butyl-4-methoxyphenol to intermediate complex **2** (0.5 mM) in acetonitrile at  $-25\text{ }^\circ\text{C}$ . The EPR data was collected at 100K.

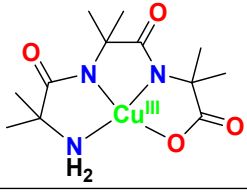
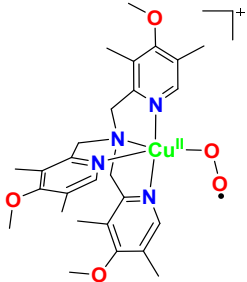
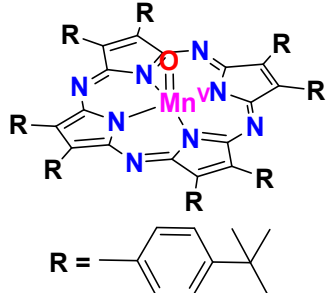
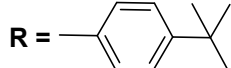
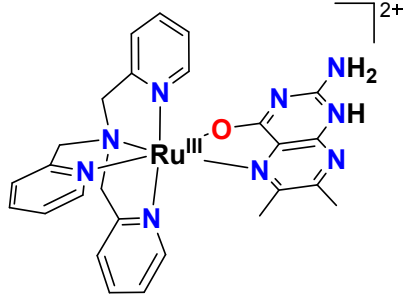
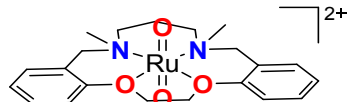


**Figure S16.** GC-mass spectrum of the reaction solution obtained upon reacting intermediate **2** with 2,6-Di-*tert*-butyl-4-methoxyphenol.

**Table S7.** Second-order-rate constants ( $k_2$ ) for the reaction of intermediate **2** with 2,6-Di-*tert*-butyl-4-methoxyphenol at different temperatures.

Temperature (K)	$k_2$ ( $M^{-1} s^{-1}$ )
248	71.15
243	53.59
238	35.29
233	25.43
228	18.61

**Table S8.** Activation parameters of different HAT type reactions.

Intermediate	Substrate	$\Delta H^\ddagger$ (Kcal mol <sup>-1</sup> )	$\Delta S^\ddagger$ (cal mol <sup>-1</sup> K <sup>-1</sup> )
$[(L\bullet)Fe^{III}(OH)]^{-a}$	2,6-Di- <i>tert</i> -butyl-4-methoxyphenol <sup>a</sup>	$7.23 \pm 0.28$	$-20.54 \pm 1.6$
	2,4-Di- <i>tert</i> -butylphenol <sup>33</sup>	$8.3 \pm 1.1$	$-27 \pm 3$
	2,6-Di- <i>tert</i> -butyl-4-methoxyphenol <sup>2</sup>	$3.6 \pm 0.6$	$-32 \pm 3$
 R = 	2,4-Di- <i>tert</i> -butylphenol <sup>34</sup>	$6.3 \pm 1.4$	$-35.6 \pm 2.3$
	2,4-6-tri- <i>tert</i> -butylphenol <sup>35</sup>	$1.6 \pm 0.2$	$-36 \pm 2$
	Phenol <sup>36</sup>	$11.3 \pm 0.8$	$-14 \pm 2$

<sup>a</sup>Present study.

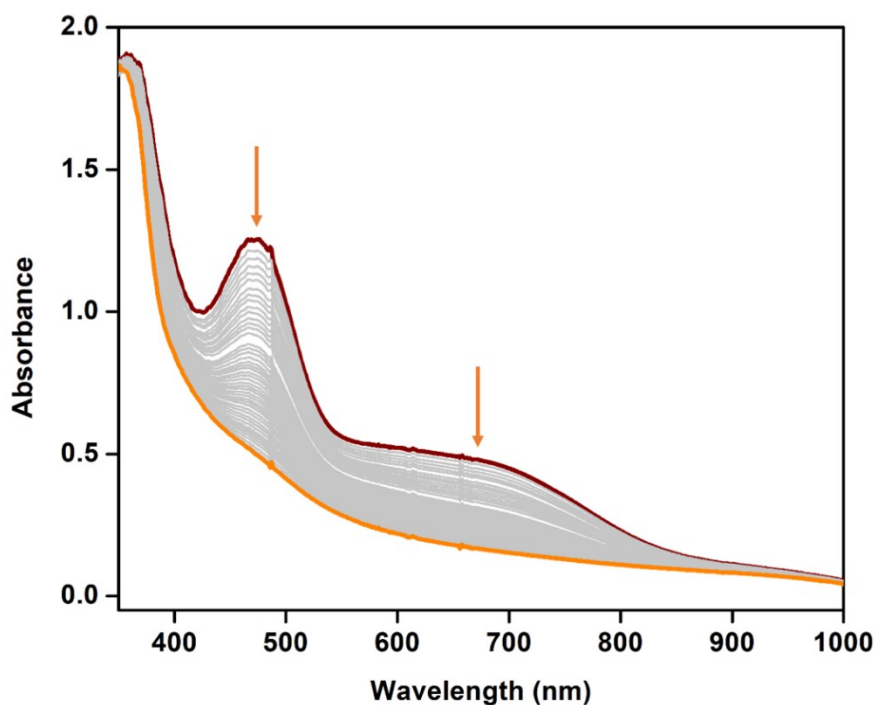


**Figure S17.** Change of single spectrum of **2** (0.32 mM) upon addition of 11.9 mM solution of 4-methyl-2,6-di-*tert*-butylphenol (4-Me-DTBP) in acetonitrile at  $-25\text{ }^{\circ}\text{C}$ .

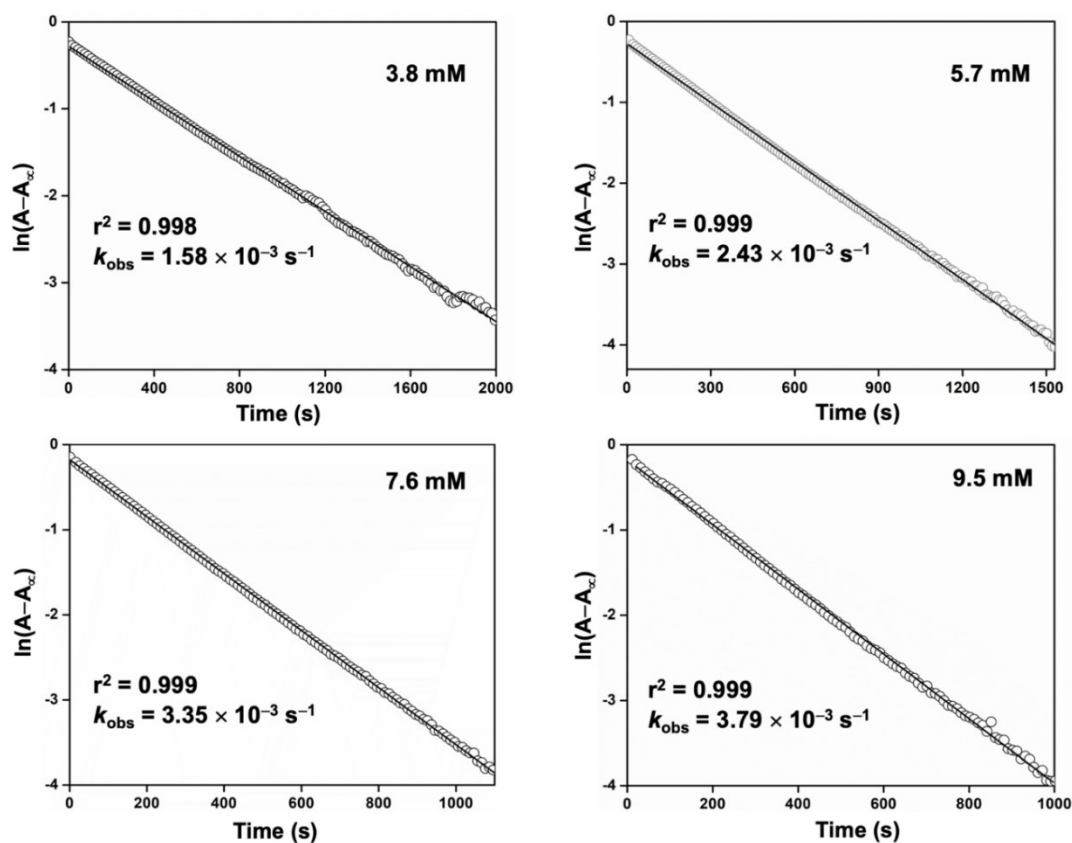


**Figure S18.** Pseudo-first-order fitting of the time trace at 470 nm for the reaction of **2** (0.32 mM) with 4-methyl-2,6-di-*tert*-butylphenol at different concentrations (3.8–9.5 mM). The reaction was studied at  $-25\text{ }^{\circ}\text{C}$ . Pseudo-first-order rate constants ( $k_{\text{obs}}$ ) were determined from the slope of the above plots.

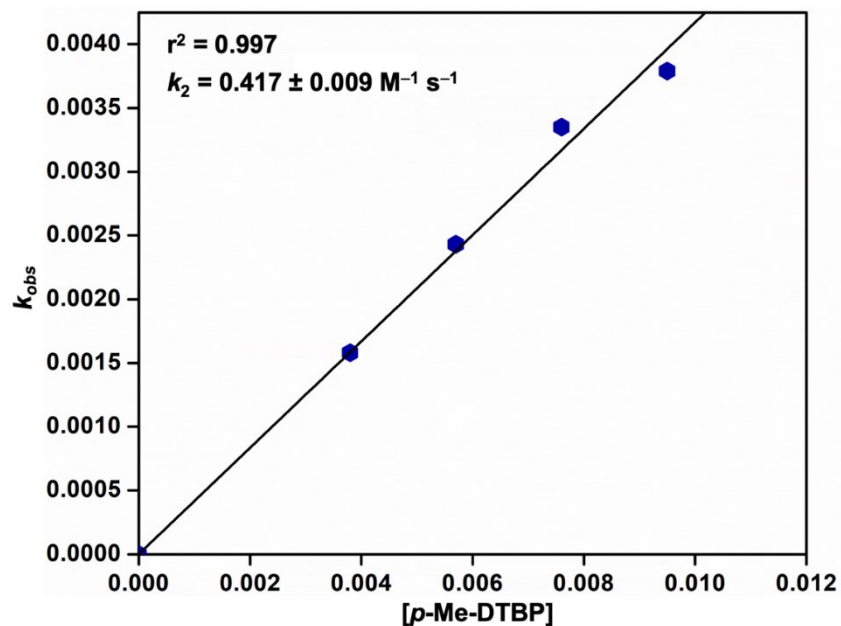


**Figure S19.** A plot of  $k_{obs}$  vs. [4-methyl-2,6-di-*tert*-butylphenol]. The  $k_{obs}$  values were obtained reacting **2** with different concentration of 4-methyl-2,6-di-*tert*-butylphenol at  $-25\text{ }^{\circ}\text{C}$  in acetonitrile. The second order-rate constant was obtained from the slope of the plot.

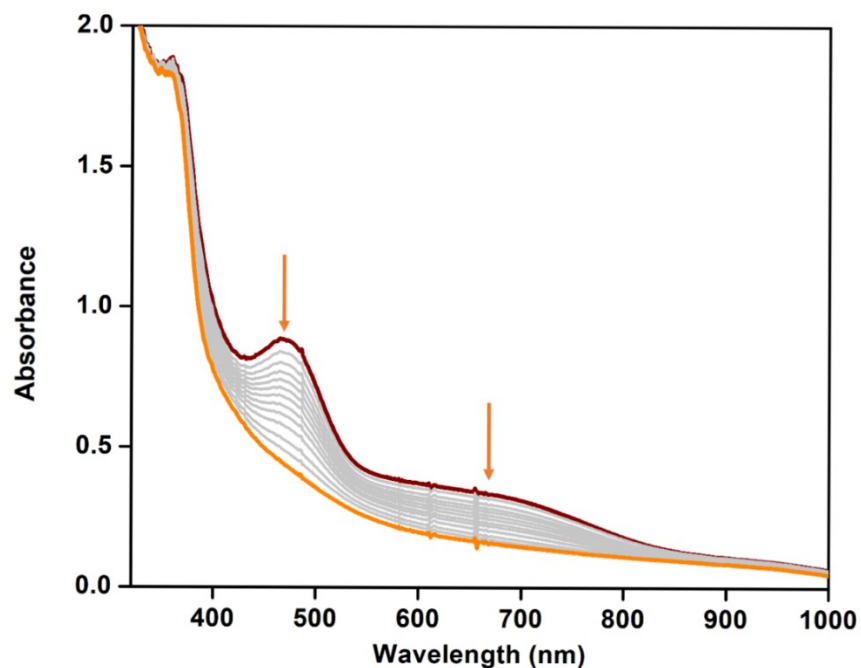


**Figure S20.** Change of single spectrum of **2** (0.25 mM) upon addition of 2.6 mM of 4-Ethyl-2,6-di-*tert*-butylphenol in acetonitrile at  $-25\text{ }^{\circ}\text{C}$ .

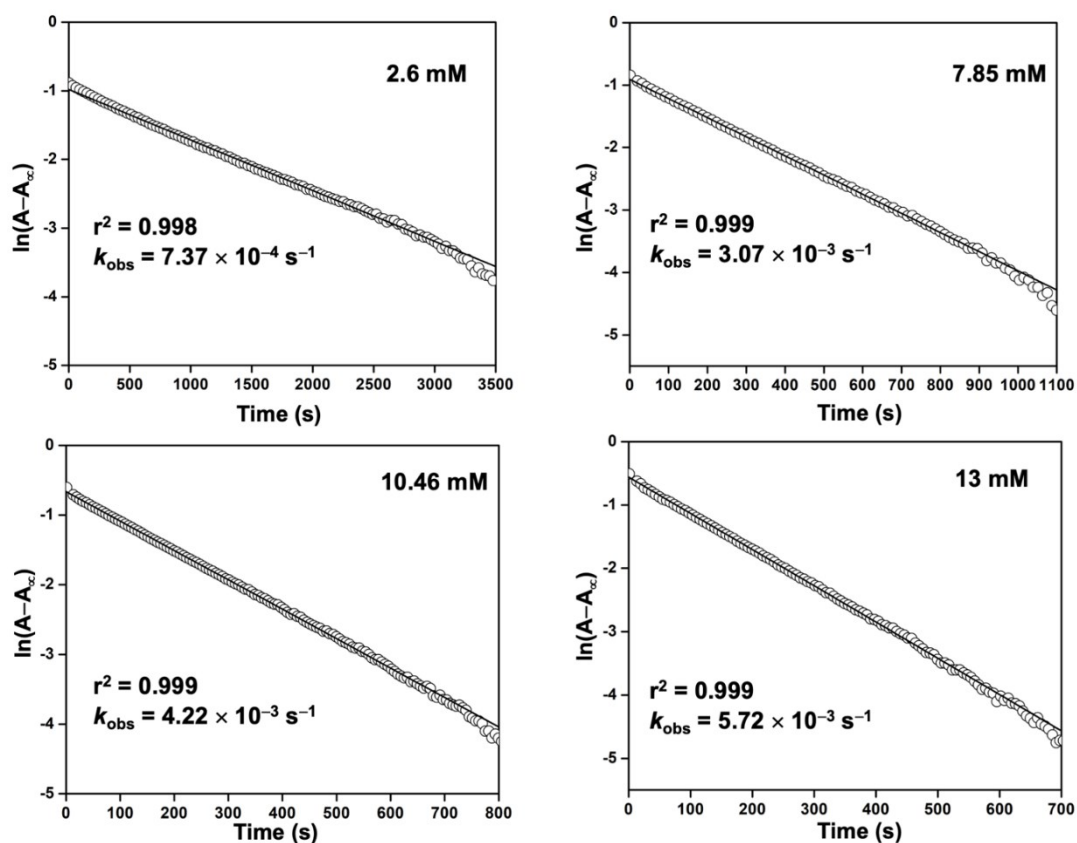


**Figure S21.** Pseudo-first-order fitting of the time trace at 470 nm for the reaction of **2** (0.25 mM) with 4-Ethyl-2,6-di-*tert*-butylphenol at different concentrations (2.6–13 mM). The reaction was studied at  $-25\text{ }^{\circ}\text{C}$ . Pseudo-first-order rate constants ( $k_{\text{obs}}$ ) were determined from the slope of the above plots.

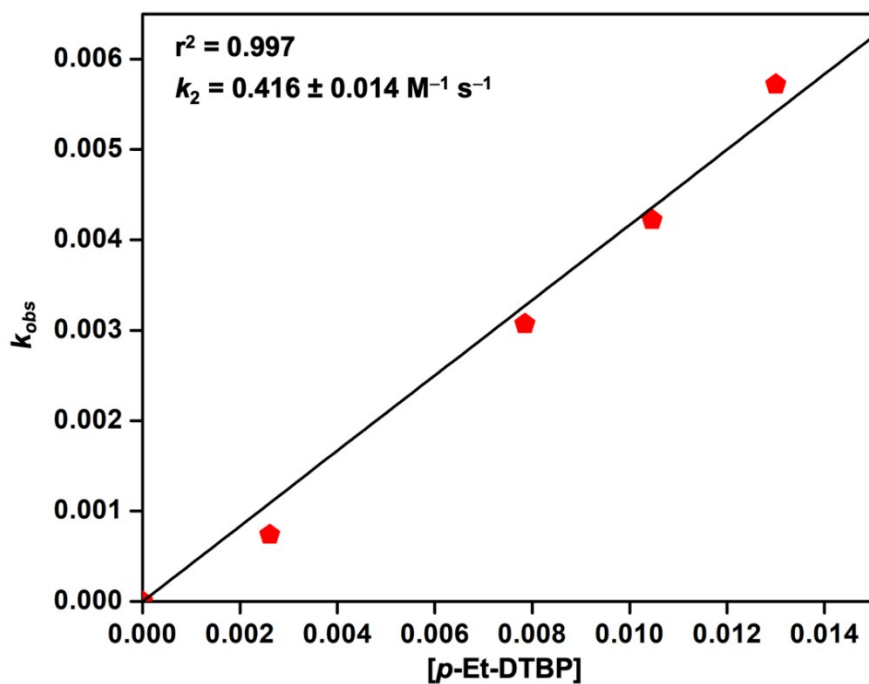


**Figure S22.** A plot of  $k_{\text{obs}}$  vs. [4-Ethyl-2,6-di-*tert*-butylphenol]. The  $k_{\text{obs}}$  values were obtained reacting **2** with different concentration of 4-Ethyl-2,6-di-*tert*-butylphenol at  $-25\text{ }^{\circ}\text{C}$  in acetonitrile. The second order-rate constant was obtained from the slope of the plot.

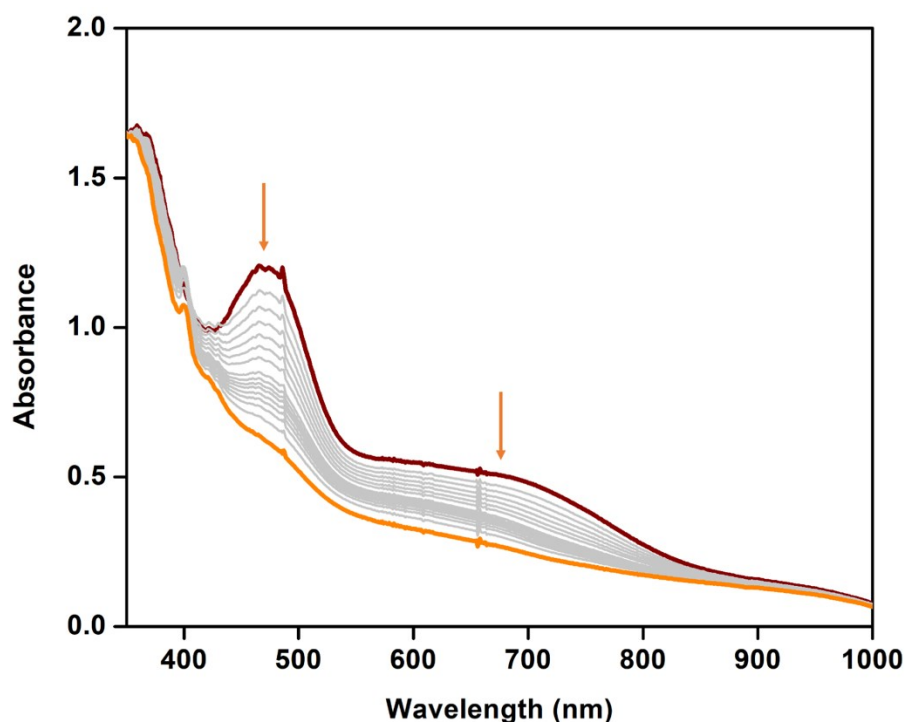


**Figure S23.** Change of single spectrum of **2** (0.32 mM) upon addition of 3.8 mM of 2,4,6-tri-*tert*-butylphenol (TTBP) in acetonitrile at  $-25\text{ }^{\circ}\text{C}$ .

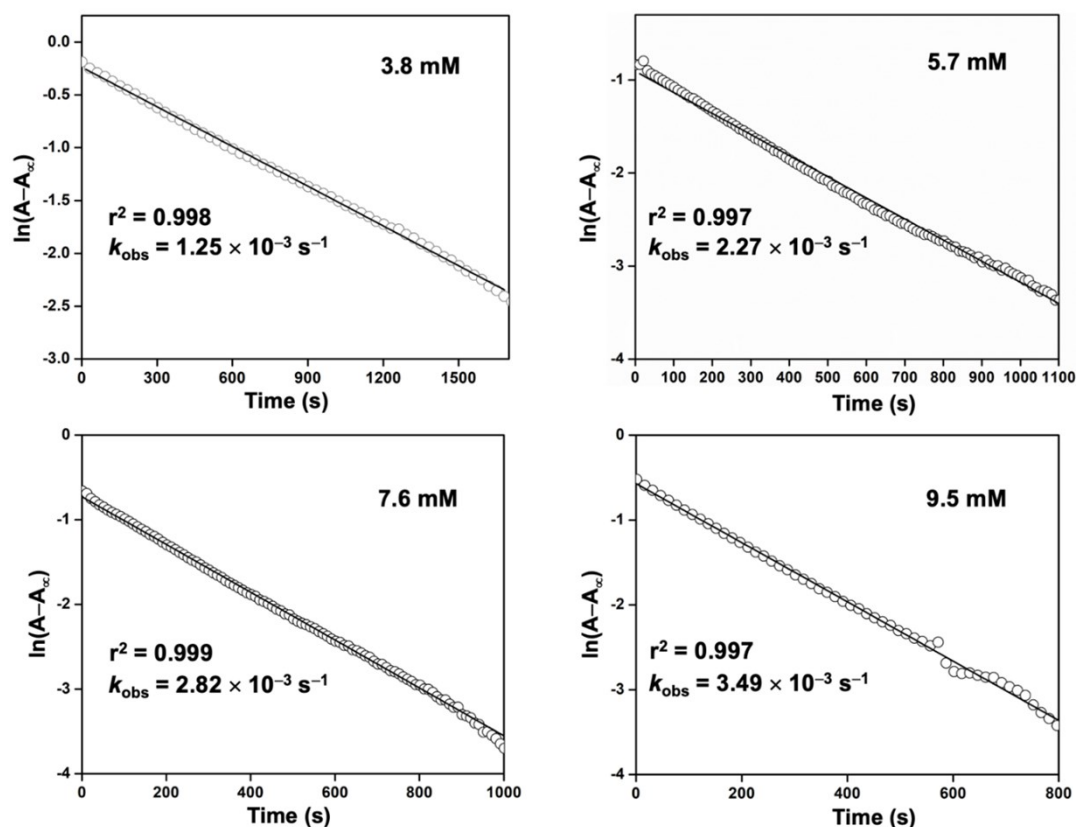


**Figure S24.** Pseudo-first-order fitting of the time trace at 470 nm for the reaction of **2** (0.32 mM) with 2,4,6-tri-*tert*-butylphenol at different concentrations (3.8–9.5 mM). The reaction was studied at  $-25\text{ }^{\circ}\text{C}$ . Pseudo-first-order rate constants ( $k_{\text{obs}}$ ) were determined from the slope of the above plots.



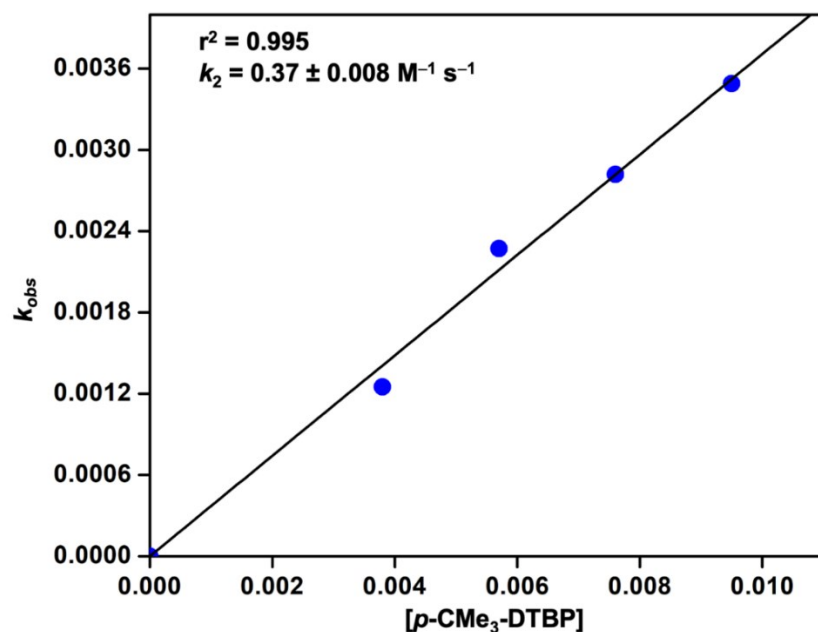


**Figure S25.** A plot of  $k_{\text{obs}}$  vs. [2,4,6-tri-*tert*-butylphenol]. The  $k_{\text{obs}}$  values were obtained reacting **2** with different concentration of 2,4,6-tri-*tert*-butylphenol at  $-25^\circ\text{C}$  in acetonitrile. The second order-rate constant was obtained from the slope of the plot.

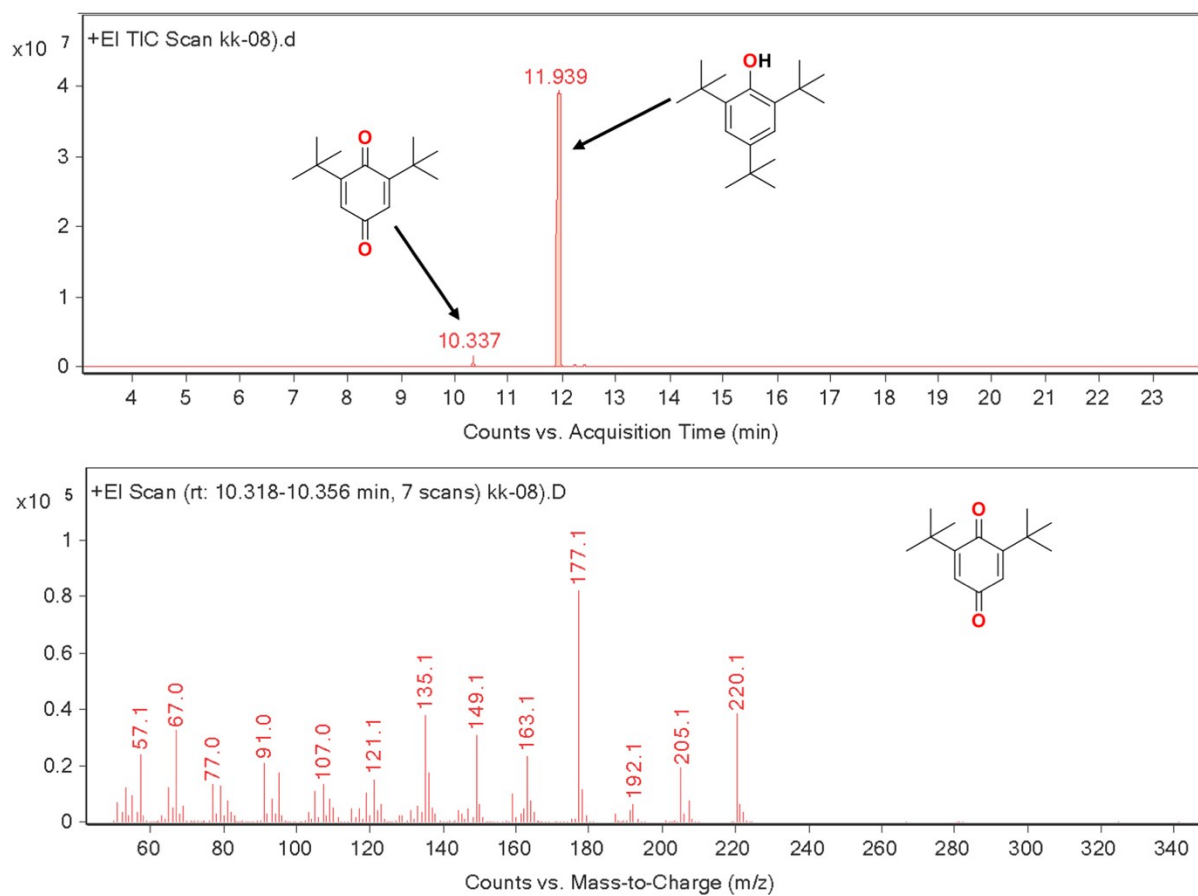


**Figure S26.** GC-mass spectrum of the reaction solution obtained upon reacting intermediate **2** with 2,4,6-tri-*tert*-butylphenol.

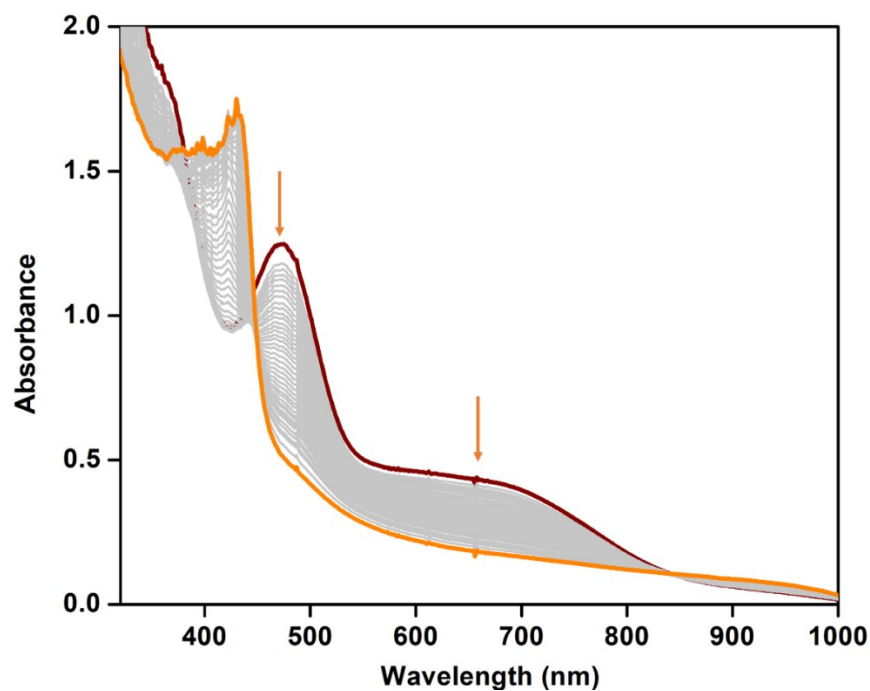


**Figure S27.** Change of single spectrum of **2** (0.32 mM) upon addition of 10.3 mM of 2,6-di-*tert*-butylphenol in acetonitrile at  $-25\text{ }^{\circ}\text{C}$ .

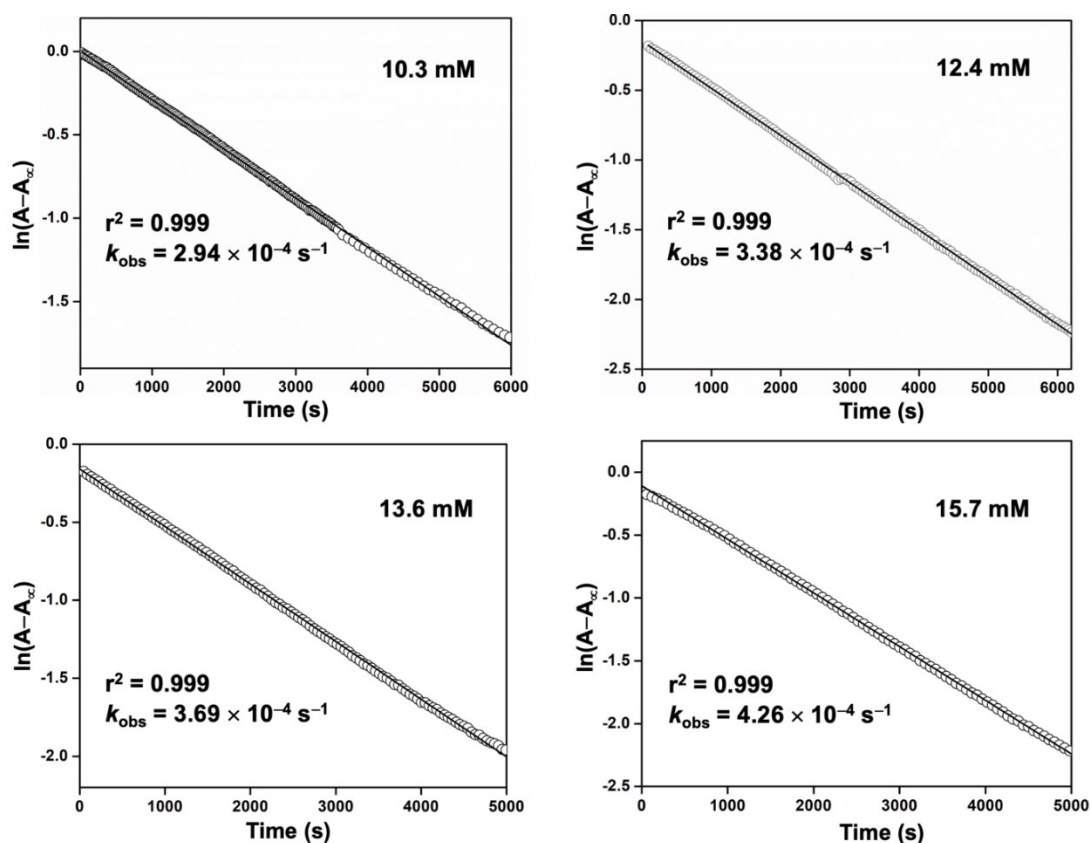


**Figure S28.** Pseudo-first-order fitting of the time trace at 470 nm for the reaction of **2** (0.32 mM) with 2,6-di-*tert*-butylphenol at different concentrations (10.3–15.7 mM). The reaction was studied at  $-25\text{ }^{\circ}\text{C}$ . Pseudo-first-order rate constants ( $k_{\text{obs}}$ ) were determined from the slope of the above plots.

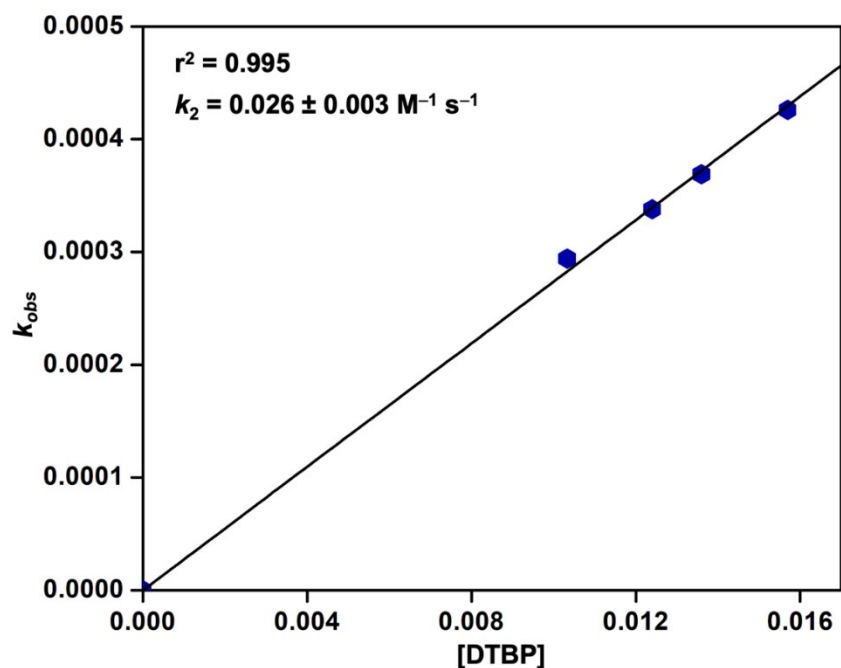


**Figure S29.** A plot of  $k_{obs}$  vs. [2, 6-di-*tert*-butylphenol]. The  $k_{obs}$  values were obtained reacting **2** with different concentration of 2, 6-di-*tert*-butylphenol at  $-25$  °C in acetonitrile. The second order-rate constant was obtained from the slope of the plot.

**Table S9.** Second order rate constant for the reaction of **2** with 4-X-2,6-di-*tert*-butylphenols (X=  $-\text{OCH}_3$ ,  $-\text{CH}_3$ ,  $-\text{C}(\text{CH}_3)_3$ ,  $-\text{H}$ ) and O–H bond dissociation energy of different phenols.<sup>37</sup>

Substrate	O–H BDE (kcal. mol <sup>-1</sup> ) <sup>a</sup>	$k_2$ (M <sup>-1</sup> s <sup>-1</sup> )	$\log k_2$
2,6-di- <i>tert</i> -butyl-4-methoxyphenol	78.31	71.15	1.85217
2,6-di- <i>tert</i> -butyl-4-methylphenol	81.02	0.417	-0.37986
2,4,6-tri- <i>tert</i> -butylphenol	81.24	0.375	-0.42597
2, 6-di- <i>tert</i> -butylphenol	82.8	0.026	-1.58503

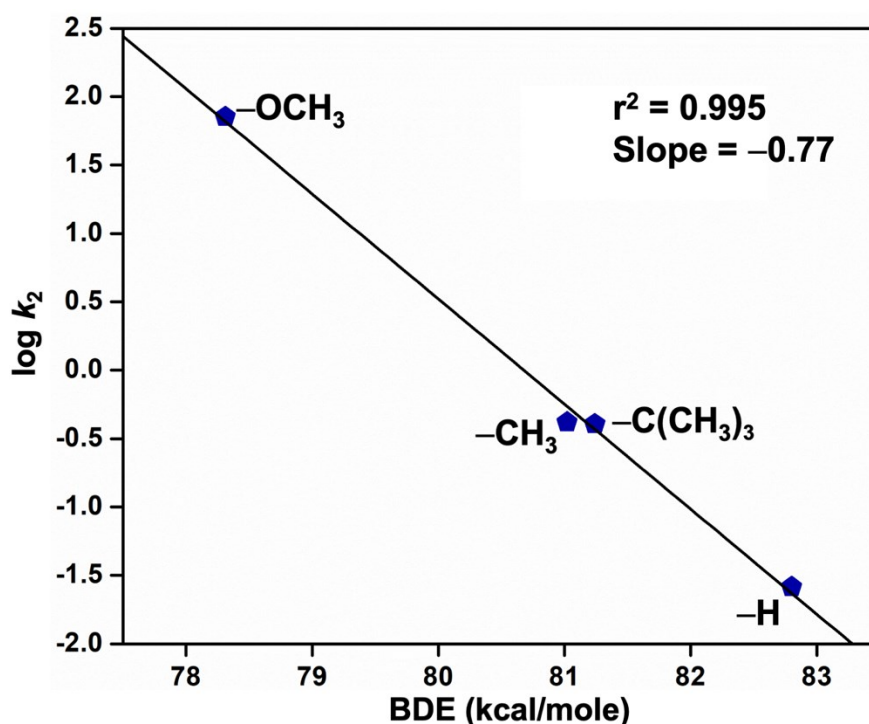


**Figure S30.** A plot of  $\log k_2$  versus bond dissociation energy of the 4-X-2,6-di-*tert*-butylphenols (X= -OCH<sub>3</sub>, -CH<sub>3</sub>, -C(CH<sub>3</sub>)<sub>3</sub>, -H).

**Table S10.** Second order rate constants for the reaction of intermediate **2** with 4-X-2,6-di-*tert*-butylphenols (X= -OCH<sub>3</sub>, -OCH<sub>3</sub>(-*d*), -CH<sub>3</sub>, -C(CH<sub>3</sub>)<sub>3</sub>, -H) and  $\sigma_p^+$  values of different *p*-substituted-2,6-di-*tert*-butylphenols.<sup>3</sup>

Phenols	$\sigma_p^+$	$k_2$ (M <sup>-1</sup> s <sup>-1</sup> )	$\log k_2$
2,6-di- <i>tert</i> -butyl-4-methoxyphenol	-0.78	71.15	1.85217
2,6-di- <i>tert</i> -butyl-4-methylphenol	-0.31	0.417	-0.37986
4-Ethyl-2,6-di- <i>tert</i> -butylphenol	-0.29	0.416	-0.38090
2,4,6-tri- <i>tert</i> -butylphenol	-0.26	0.375	-0.42597
2, 6-di- <i>tert</i> -butylphenol	0	0.026	-1.58503

**Table S11.** Second order rate constants for the reaction of intermediate **2** with 4-X-2,6-di-*tert*-butylphenols (X= -OCH<sub>3</sub>, -OCH<sub>3</sub>(-*d*), -CH<sub>3</sub>, -CH<sub>2</sub>CH<sub>3</sub>, -C(CH<sub>3</sub>)<sub>3</sub>, -H) and oxidation potential of different *p*-substituted-2,6-di-*tert*-butylphenols.<sup>2</sup>

Phenols	$E_{Ox}/V$ $Fc/Fc^{+a}$	vs.	$k_2$ (M <sup>-1</sup> s <sup>-1</sup> )	T/K	$(RT/F)\ln k_2$
2,6-di- <i>tert</i> -butyl-4-methoxyphenol	0.526		71.15	248	0.0911
2,6-di- <i>tert</i> -butyl-4-methoxyphenol- <i>d</i>	0.585		51.14	248	0.08404
2,6-di- <i>tert</i> -butyl-4-methylphenol	0.81		0.417	248	-0.01868
4-Ethyl-2,6-di- <i>tert</i> -butylphenol	0.88		0.416	248	-0.01869
2,4,6-tri- <i>tert</i> -butylphenol	0.927		0.375	248	-0.02095
2, 6-di- <i>tert</i> -butylphenol	1.074		0.026	248	-0.07796

<sup>a</sup> $E_{Ox}$  values are taken from ref. [2]

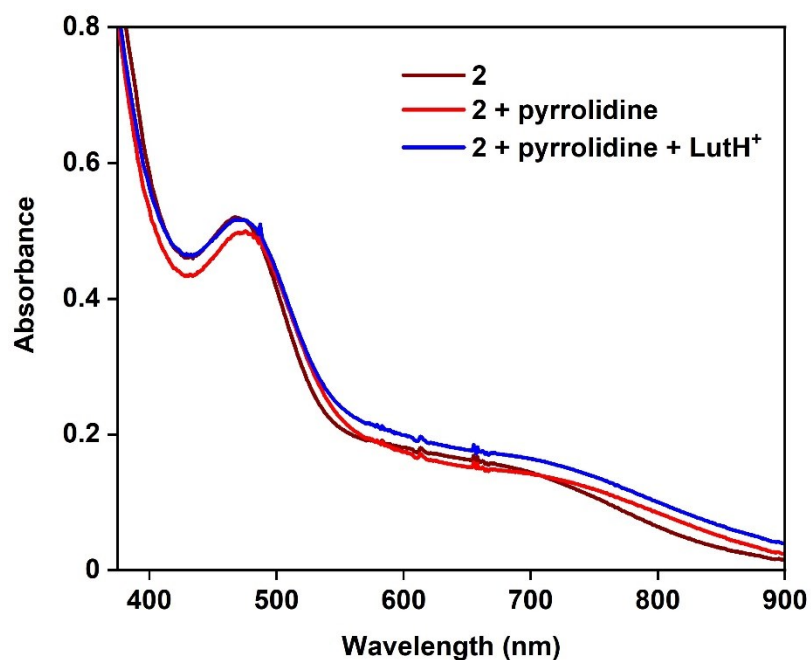
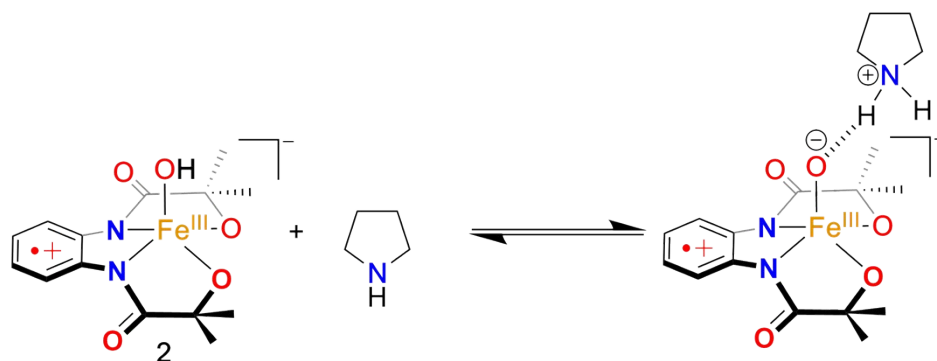


**Figure S31.** UV-Vis spectral change of **2** (0.12 mM) observed upon addition of 1 equiv. of pyrrolidine and followed by addition of 1 equiv. of 2,6-lutidinium triflate (LutH<sup>+</sup>OTf<sup>-</sup>) in acetonitrile at -25 °C.



**Scheme S1.** Proposed reaction for the reaction of **2** with pyrrolidine.

**Appendix, Calculation 1:** B3LYP-def2-TZVP, D3BJ

Fe	6.907664	7.430969	12.820624
O	5.269769	7.110987	11.733571
O	6.854397	9.282996	13.277804
O	8.300931	7.560673	11.546128
N	6.229031	7.191895	14.596013
O	5.433074	8.345912	16.431830
N	7.622629	5.679532	13.134257
O	9.260181	4.205093	12.437224
C	8.647969	5.284053	12.363824
C	9.024792	6.370083	11.325524
C	10.524441	6.669954	11.451755
H	10.797670	7.435905	10.723171
H	11.126066	5.778793	11.266222
H	10.751756	7.048915	12.451054
C	8.726477	5.820665	9.921564
H	7.657772	5.623162	9.812389

H	9.275420	4.896427	9.732889
H	9.022930	6.562651	9.176402
C	7.063753	5.018644	14.235878
C	6.275377	5.871704	15.058106
C	5.869636	8.294720	15.270736
C	6.057348	9.563064	14.404664
C	4.656588	10.033577	13.970946
H	4.743391	10.966096	13.407788
H	4.010066	10.204389	14.833994
H	4.196328	9.286729	13.322293
C	6.730367	10.651473	15.245145
H	7.711007	10.315899	15.589746
H	6.127647	10.909309	16.116557
H	6.863832	11.544990	14.631915
C	5.631375	5.351035	16.178811
H	5.037816	6.007878	16.795231
C	5.757354	3.995677	16.488408
H	5.242840	3.596281	17.353893
C	6.535346	3.163805	15.691915
H	6.637581	2.114445	15.941287
C	7.190348	3.670761	14.566947
H	7.793740	3.030233	13.942478
H	4.526651	7.187323	12.342337

**Calculation 2:** BP86-def2-TZVP, D3BJ

Fe	7.082691	7.483649	12.923952
O	5.608850	7.223245	11.608048
O	6.980821	9.321438	13.404278
O	8.586269	7.638262	11.788995
N	6.235147	7.192835	14.608133
O	5.075040	8.295421	16.302712
N	7.735480	5.713057	13.233160
O	9.202878	4.121753	12.366710
C	8.692448	5.265753	12.388375
C	9.087321	6.374037	11.374739
C	10.615514	6.448654	11.272030
H	10.897981	7.200078	10.519842
H	11.042742	5.478254	10.982447
H	11.046820	6.744573	12.240146
C	8.463520	5.995027	10.016639
H	7.368032	6.019692	10.108842
H	8.782532	4.993775	9.689815
H	8.771405	6.728728	9.255891
C	7.138203	5.033905	14.301716
C	6.280977	5.873752	15.082447
C	5.720701	8.280814	15.229739
C	6.023559	9.571231	14.420014
C	4.699013	10.043697	13.787141
H	4.866577	10.988781	13.248147
H	3.920891	10.202455	14.548553
H	4.348277	9.291635	13.065543
C	6.568989	10.640595	15.377503
H	7.521706	10.305839	15.813525
H	5.859848	10.840148	16.192672
H	6.747357	11.573946	14.823652

C	5.616085	5.343005	16.197547
H	4.971250	5.992837	16.785060
C	5.794461	3.994141	16.539139
H	5.272144	3.587110	17.406973
C	6.632902	3.174471	15.778135
H	6.766832	2.125693	16.050079
C	7.308326	3.688300	14.661617
H	7.969179	3.064123	14.063703
H	4.788590	7.221985	12.133659

**Calculation 3:** BLYP-def2-TZVP,D3BJ

Fe	7.062471	7.484984	12.904498
O	5.561000	7.224405	11.591344
O	6.958464	9.336312	13.394554
O	8.571563	7.635332	11.750933
N	6.219910	7.191574	14.611898
O	5.078093	8.298974	16.323243
N	7.727433	5.699041	13.218365
O	9.214620	4.113084	12.361925
C	8.692519	5.255606	12.377730
C	9.093827	6.364280	11.354336
C	10.629556	6.458104	11.277849
H	10.914002	7.214760	10.534886
H	11.072769	5.496099	10.992491
H	11.038943	6.755048	12.252819
C	8.498252	5.968352	9.980265
H	7.403595	5.966022	10.049189
H	8.844950	4.975383	9.663617
H	8.803360	6.705078	9.224374
C	7.131962	5.023983	14.298570
C	6.276148	5.865842	15.085355
C	5.713371	8.281721	15.240251
C	6.008849	9.583526	14.430521
C	4.674279	10.070416	13.812067
H	4.843686	11.012429	13.272625
H	3.910667	10.236592	14.583574
H	4.305264	9.324134	13.097495
C	6.576475	10.650777	15.388736
H	7.526828	10.304703	15.815720
H	5.877887	10.858358	16.208099
H	6.760984	11.579940	14.833913
C	5.618668	5.332777	16.206778
H	4.977504	5.977860	16.797723
C	5.801248	3.982897	16.551206
H	5.286259	3.577947	17.421539
C	6.637092	3.162243	15.785164
H	6.774566	2.116231	16.056877
C	7.304824	3.677020	14.661705
H	7.959757	3.051378	14.064556
H	4.739714	7.263483	12.114526

**Calculation 4:** PBE-SVP D3BJ

Fe	7.172343	7.547831	12.999769
O	5.695605	7.396426	11.679070

O	7.106516	9.369390	13.527187
O	8.735408	7.672806	11.923458
N	6.317769	7.231298	14.692575
O	5.117720	8.345119	16.358909
N	7.728352	5.726549	13.246413
O	9.111315	4.103498	12.292180
C	8.663090	5.267653	12.372029
C	9.099755	6.413498	11.407671
C	10.622448	6.346598	11.218116
H	10.947546	7.080727	10.452516
H	10.934411	5.330709	10.903412
H	11.133031	6.590234	12.172949
C	8.359135	6.164854	10.071761
H	7.278558	6.342586	10.258845
H	8.523024	5.135717	9.688336
H	8.711651	6.890996	9.308475
C	7.120035	5.043356	14.303660
C	6.315585	5.904649	15.131883
C	5.780153	8.322556	15.298826
C	6.062752	9.599083	14.446829
C	4.752603	9.910222	13.683773
H	4.863914	10.864759	13.125915
H	3.882833	9.997061	14.368122
H	4.588741	9.089520	12.953521
C	6.441345	10.751541	15.388116
H	7.416106	10.536612	15.873569
H	5.676093	10.880749	16.179318
H	6.539512	11.698126	14.818012
C	5.656469	5.371603	16.259725
H	5.060635	6.050188	16.883906
C	5.782720	4.000981	16.561985
H	5.264171	3.590047	17.442891
C	6.566733	3.160343	15.752901
H	6.661972	2.090441	15.998483
C	7.239648	3.675311	14.627018
H	7.867112	3.041640	13.986648
H	5.294552	6.541420	11.932549

**Calculation 5:** BP86- 6-31+G\*, D3BJ

Fe	7.044911	7.464086	12.896918
O	5.568932	7.178826	11.582902
O	6.911590	9.307018	13.351515
O	8.552555	7.629945	11.763316
N	6.206309	7.181632	14.589388
O	5.091360	8.287281	16.318740
N	7.716653	5.701826	13.213235
O	9.246090	4.131617	12.403995
C	8.705143	5.264719	12.393439
C	9.092974	6.369440	11.369678
C	10.622498	6.479633	11.293795
H	10.903531	7.240899	10.548346
H	11.079239	5.520222	11.005604
H	11.035038	6.780522	12.270585



C	8.501806	5.963279	10.002696
H	7.402751	5.964968	10.067628
H	8.844772	4.963454	9.689287
H	8.808878	6.693456	9.235515
C	7.128542	5.022872	14.293847
C	6.266218	5.860951	15.075411
C	5.710130	8.273583	15.226786
C	6.000127	9.567412	14.413573
C	4.660094	10.078405	13.842310
H	4.831550	11.008421	13.275598
H	3.929488	10.283392	14.641505
H	4.227935	9.332928	13.155477
C	6.610331	10.619180	15.355137
H	7.572008	10.261251	15.755691
H	5.938715	10.836665	16.199742
H	6.790930	11.553146	14.799222
C	5.607014	5.330104	16.197866
H	4.957911	5.977058	16.787610
C	5.798090	3.981122	16.546509
H	5.280706	3.573694	17.420223
C	6.642034	3.162407	15.784171
H	6.786431	2.113835	16.061186
C	7.310815	3.677453	14.659700
H	7.975708	3.051670	14.064318
H	4.731555	7.388328	12.038851

**Calculation 6:** B3LYP- 6-31+G\*, D3BJ

Fe	7.083952	7.468623	12.914331
O	5.673025	7.171343	11.556931
O	6.873400	9.299117	13.358954
O	8.647816	7.637318	11.841198
N	6.208164	7.169266	14.595353
O	5.040544	8.250447	16.281410
N	7.758325	5.695987	13.235600
O	9.379889	4.200662	12.520804
C	8.781116	5.290061	12.457635
C	9.122441	6.376711	11.400296
C	10.634647	6.450387	11.181393
H	10.853455	7.208362	10.423289
H	11.035621	5.494099	10.836925
H	11.146530	6.731406	12.106320
C	8.416315	5.983397	10.084947
H	7.334047	6.035329	10.218535
H	8.695504	4.977051	9.757413
H	8.696725	6.690544	9.297639
C	7.163774	5.024726	14.315124
C	6.269990	5.847349	15.066706
C	5.679592	8.243778	15.212705
C	5.967702	9.544441	14.418314
C	4.633246	10.076995	13.865049
H	4.813096	10.995912	13.299147
H	3.924697	10.297081	14.668315

H	4.174841	9.347916	13.190112
C	6.586119	10.577064	15.369054
H	7.520216	10.194125	15.790358
H	5.911134	10.823307	16.191838
H	6.809252	11.491795	14.812533
C	5.569890	5.307646	16.152187
H	4.887413	5.936276	16.706038
C	5.776696	3.972030	16.517467
H	5.231819	3.558585	17.360679
C	6.671856	3.176474	15.804828
H	6.837857	2.144674	16.098429
C	7.366924	3.697606	14.706060
H	8.058925	3.083600	14.146830
H	4.854803	7.605211	11.830572

## References

1. E. S. Jang, C. L. McMullin, M. Kass, K. Meyer, T. R. Cundari and T. H. Warren, *J. Am. Chem. Soc.*, 2014, **136**, 10930-10940.
2. J. Y. Lee, R. L. Peterson, K. Ohkubo, I. Garcia-Bosch, R. A. Himes, J. Woertink, C. D. Moore, E. I. Solomon, S. Fukuzumi and K. D. Karlin, *J. Am. Chem. Soc.*, 2014, **136**, 9925-9937.
3. C. Hansch, A. Leo and R. W. Taft, *Chem. Rev.*, 1991, **91**, 165-195.
4. S. K. Sur, *J. Magn. Reson.*, 1989, **82**, 169-173.
5. G. A. Bain and J. F. Berry, *J. Chem. Educ.*, 2008, **85**, 532-536.
6. X. Lu, X.-X. Li, M. S. Seo, Y.-M. Lee, M. Clemancey, P. Maldivi, J.-M. Latour, R. Sarangi, S. Fukuzumi and W. Nam, *J. Am. Chem. Soc.*, 2019, **141**, 80-83.
7. APEX II 2009 Ed.; Bruker Analytical X-ray Systems Inc.: Madison, WI, 2009
8. G. M. Sheldrick, *Acta Crystallogr., Sect. A Found. Crystallogr.*, 2008, **A64**, 112-122.
9. M. N. Burnett and C. K. Johnson, ORTEP-III, Oak Ridge Thermal Ellipsoid Plot Program for Crystal Structure Illustrations, Report ORNL-6895, Oak Ridge National Laboratory, Oak Ridge, TN, USA, 1996
10. C. F. Macrae, I. J. Bruno, J. A. Chisholm, P. R. Edgington, P. McCabe, E. Pidcock, L. Rodriguez-Monge, R. Taylor, J. van de Streek and P. A. Wood, *J. Appl. Crystallogr.*, 2008, **41**, 466-470.
11. M. Gupta, Y. Kumar, A. Tayal, N. Pandey, W. Caliebe and J. Stahn, *SN Applied Sciences*, 2019, **2**, 41.
12. B. Ravel and M. Newville, *J. Synchrotron Rad.*, 2005, **12**, 537-541.
13. J. J. Rehr and R. C. Albers, *Rev. Mod. Phys.*, 2000, **72**, 621-654.
14. D. C. Koningsberger and R. Prins, *X Ray Absorption: Principles, Applications, Techniques of EXAFS, SEXAFS and XANES*, John Wiley & Sons, 1988.
15. M. Wojdyr, *J. Appl. Crystallogr.*, 2010, **43**, 1126-1128.
16. S. Pattanayak, A. J. Jasniewski, A. Rana, A. Draksharapu, K. K. Singh, A. Weitz, M. Hendrich, L. Que, A. Dey and S. Sen Gupta, *Inorg. Chem.*, 2017, **56**, 6352-6361.
17. F. Neese, *Wiley Interdisciplinary Reviews: Computational Molecular Science*, 2012, **2**, 73-78.
18. A. D. Becke, *J. Chem. Phys.*, 1993, **98**, 5648-5652.
19. P. J. Stephens, F. J. Devlin, C. F. Chabalowski and M. J. Frisch, *The Journal of Physical Chemistry*, 1994, **98**, 11623-11627.
20. F. Weigend and R. Ahlrichs, *Phys. Chem. Chem. Phys.*, 2005, **7**, 3297-3305.
21. S. Grimme, J. Antony, S. Ehrlich and H. Krieg, *J. Chem. Phys.*, 2010, **132**, 154104.

22. S. Grimme, S. Ehrlich and L. Goerigk, *J. Comput. Chem.*, 2011, **32**, 1456-1465.
23. A. D. Becke, *Physical Review A*, 1988, **38**, 3098-3100.
24. J. P. Perdew, *Physical Review B*, 1986, **33**, 8822-8824.
25. C. Lee, W. Yang and R. G. Parr, *Physical Review B*, 1988, **37**, 785-789.
26. R. Krishnan, J. S. Binkley, R. Seeger and J. A. Pople, *J. Chem. Phys.*, 1980, **72**, 650-654.
27. P. Graf, E. L. Mehler, A. D. McLean and G. S. Chandler, *J. Chem. Phys.*, 1982, **76**, 1593-1594.
28. L. A. Curtiss, P. C. Redfern, V. Rassolov, G. Kedziora and J. A. Pople, *J. Chem. Phys.*, 2001, **114**, 9287-9295.
29. M. J. Frisch, J. A. Pople and J. S. Binkley, *J. Chem. Phys.*, 1984, **80**, 3265-3269.
30. L. A. Curtiss, M. P. McGrath, J. P. Blaudeau, N. E. Davis, R. C. B. Jr. and L. Radom, *J. Chem. Phys.*, 1995, **103**, 6104-6113.
31. V. Barone and M. Cossi, *J. Phys. Chem. A*, 1998, **102**, 1995-2001.
32. S. Kossmann and F. Neese, *J. Chem. Theory Comput.*, 2010, **6**, 2325-2338.
33. M. A. Lockwood, T. J. Blubaugh, A. M. Collier, S. Lovell and J. M. Mayer, *Angew. Chem., Int. Ed.*, 1999, **38**, 225-227.
34. E. Lansky David and P. Goldberg David, *Inorg Chem*, 2006, **45**, 5119-5125.
35. S. Miyazaki, T. Kojima, J. M. Mayer and S. Fukuzumi, *J. Am. Chem. Soc.*, 2009, **131**, 11615-11624.
36. D. T. Y. Yiu, M. F. W. Lee, W. W. Y. Lam and T.-C. Lau, *Inorg. Chem.*, 2003, **42**, 1225-1232.
37. M. Lucarini, P. Pedrielli, G. F. Pedulli, S. Cabiddu and C. Fattuoni, *J. Org. Chem.*, 1996, **61**, 9259-9263.